

In-vitro and in-silico studies of annelated 1,4,7,8-tetrahydroazocine ester derivatives as nanomolar selective inhibitors of human butyrylcholinesterase

Modesto de Candia^{a,2}, Alexander A. Titov^{b,2}, Antonio Viayna^{c,2}, Larisa N. Kulikova^b, Rosa Purgatorio^a, Brigida Piergiovanni^{a,1}, Mauro Niso^a, Marco Catto^a, Leonid G. Voskressensky^b, F. Javier Luque^c, Cosimo D. Altomare^{a,*}

^a Department of Pharmacy-Pharmaceutical Sciences, University of Bari Aldo Moro, Via E. Orabona 4, 70125, Bari, Italy

^b Organic Chemistry Department, Peoples' Friendship University of Russia (RUDN University), 6 Miklukho-Maklaya St, Moscow, 117198, Russia

^c Department of Nutrition, Food Science and Gastronomy, Faculty of Pharmacy and Food Sciences, Institute of Biomedicine (IBUB) and Institute of Theoretical and Computational Chemistry (ITCUB), University of Barcelona, Av. Prat de la Riba 171, E-08921, Santa Coloma de Gramenet, Spain

ARTICLE INFO

Keywords:
Butyrylcholinesterase
Tetrahydroazocine
Inhibition
Selectivity
Drug design

ABSTRACT

Based on previous finding showing 2,3,6,11-tetrahydro-1*H*-azocino[4,5-*b*]indole as suitable scaffold of novel inhibitors of acetylcholinesterase (AChE), a main target of drugs for the treatment of Alzheimer's disease and related dementias, herein we investigated diverse newly and previously synthesized β -enamino esters (and ketones) derivatives of 1,4,7,8-tetrahydroazocines (and some azonines) fused with benzene, 1*H*-indole, 4*H*-chromen-4-one and pyrimidin-4(3*H*)-one. Twenty derivatives of diversely annelated eight-to-nine-membered azaheterocyclic ring, prepared through domino reaction of the respective tetrahydropyridine and azepine with activated alkynes, were assayed for the inhibitory activity against AChE and butyrylcholinesterase (BChE). As a major outcome, compound **7c**, an alkylamino derivative of tetrahydropyrimido[4,5-*d*]azocine, was found to be a highly potent BChE-selective inhibitor, which showed a noncompetitive/mixed-type inhibition mechanism against human BChE with single digit nanomolar inhibition constant ($K_i = 7.8 \pm 0.2$ nM). The four-order magnitude BChE-selectivity of **7c** clearly reflects the effect of lipophilicity upon binding to the BChE binding cavity. The ChEs' inhibition data, interpreted by chemoinformatic tools and an in-depth in-silico study (molecular docking combined with molecular dynamics calculations), not only highlighted key structural factors enhancing inhibition potency and selectivity toward BChE, but also shed light on subtle differences distinguishing the binding sites of equine BChE from the recombinant human BChE. Compound **7c** inhibited P-glycoprotein with IC_{50} of 0.27 μ M, which may support its ability to permeate blood-brain barrier, and proved to be no cytotoxic in human liver cancer cell line (HepG2) at the BChE bioactive concentrations. Overall, the biological profile allows us to envision **7c** as a promising template to improve design and development of BChE-selective ligands of pharmaceutical interest, including inhibitors and fluorogenic probes.

1. Introduction

Medium-sized azaheterocycles (typically 8-to-11-membered rings) have widespread interest in organic synthesis [1,2] and biology [3]. Indeed, such heterocyclic rings are found as subunits or core structures in natural and bioactive molecules [4], including medicinal products, whereas on the other hand they often can serve as key intermediates in

the synthesis of bicyclic compounds by selective transformations (e.g., transannular ring-contractions, cycloadditions) [5]. These molecular frameworks, particularly annelated 8-to-10-membered azaheterocycles, have long drawn our attention as potential scaffolds for developing novel acetylcholinesterase (AChE)-based multitarget-directed ligands (MTDLs) for treating Alzheimer's disease (AD) and other neurodegenerative syndromes.

* Corresponding author.

E-mail address: cosimodamiano.altomare@uniba.it (C.D. Altomare).

¹ Present address: Dompé Farmaceutici S.p.A., Via Santa Lucia, 6, 20122 Milano.

² Equally contributing authors.

Several years ago, some of us reported β -enamino ester (COOMe, COOEt) derivatives of 2,3,6,11-tetrahydro-1*H*-azocino[4,5-*b*]indole (see structure **1** in Fig. 1) and 2,3,6,7-tetrahydro-1*H*-azocino[5,4-*b*]indole (see structure **3** in Scheme 2), which had been synthesized through efficient 6 \rightarrow 8 membered ring expansion domino reactions. Some of them showed AChE inhibitory activity (e.g., **1a** in Table 1) in the low (single digit) micromolar range [6]. More recently, a series of fused ten-membered azaheterocyclic scaffold of compounds, namely allene 3-benzazecines, were found to exhibit micromolar AChE inhibitory potency [7,8] or substrates in the diastereoselective synthesis of *N*-bridged cyclopenta[*a*]indene derivatives achieving nanomolar butyrylcholinesterase (BChE) inhibition potency [9]. Regarding the tetrahydroazocine-bearing β -enamino ester derivatives, previous enzyme inhibition assays [6] suggested as a trend that increasing size and lipophilicity of the substituents on the scaffold (**1a** and **1b** in Fig. 1) may increase the inhibition of BChE, and not AChE (Table 1). Using this medium-sized heterocyclic scaffold we wanted to further investigate the molecular factors favoring selectivity toward BChE, which may represent a drug target for AD and other diseases.

BChE (EC 3.1.1.8), also known as plasma cholinesterase or pseudo-cholinesterase, is an abundant serine hydrolase, widely distributed in mammalian tissues with the highest levels detected in plasma and liver [10,11]. BChE exists in human plasma mainly as glycosylated soluble homotetramers with a molecular weight of 340 kDa, but a small portion occurs as homodimers and monomers [12]. The main function of BChE consists in hydrolyzing acetylcholine, particularly as a compensative action in the advanced stages of neurodegenerative diseases such as AD. Indeed, cholinesterase inhibitors, which increase the availability of neurotransmitters at brain cholinergic synapses, are used clinically as the mainstay of AD therapy [13]. BChE was also found in amyloid plaques and neurofibrillary tangles, which suggests that the protein may play a role in the pathogenesis of AD [14]. BChE is more abundant in plasma, where it serves as defense against AChE toxic inhibitors such as organophosphate pesticides and nerve agents acting at the neuromuscular junction [15].

Although a comprehensive understanding of the biological roles remains to be elucidated, BChE may work as a multifaceted protein. In blood and plasma, BChE hydrolase activity leads to degradation of all ester chemicals of sufficient size to fit into the enzyme active site pocket, including the anesthetics succinylcholine and procaine, as well as illicit drugs like cocaine and heroin [16,17]. Recently, it was further suggested

that BChE might interact with plasma proteins and forms much larger complexes than predicted from the molecular weight of the BChE tetramer. Binding studies revealed that BChE interacts with several proteins in human serum, such as ApoA-I and HDL in a more stable than transient mode, thus suggesting a role in metabolism regulation [10].

Research over the past two decades revealed new roles for BChE. A relevant BChE activity, correlated with microglial activation, has been found in multiple sclerosis white matter lesions associated with myelin, thus suggesting a role of BChE in degradation of lipid thioesters constituting myelin [18]. Most recently, it has been reported that BChE hydrolyzes the hormone ghrelin, thus affecting metabolism, as well as aggression and social stress in animal model [19].

The preceding evidence suggests that the identification of potent, selective inhibitors of BChE can be expected to be valuable for gaining insight into the roles mediated by this enzyme. Taking advantage of the elongated shape of the binding cavity, the availability of potent inhibitors could pave the way to the design of hybrid compounds containing fluorescent moieties, which in turn could be used for monitoring real-time BChE levels, gaining better understanding of its roles in physiological processes, and diagnose anomalous BChE levels associated to the progression of specific diseases.

In this context, this study reports a combined in-vitro and in-silico study about a class of annelated tetrahydroazocine ester derivatives as BChE-selective inhibitors. Herein, we investigated diverse newly (**3a-e** and **10a-b** in Schemes 2 and 3, respectively) and previously synthesized β -enamino esters (and ketones) derivatives of 1,4,7,8-tetrahydroazocines (and some azonines) fused with benzene, 1*H*-indole (in two different fusion isomers), 4*H*-chromen-4-one and pyrimidin-4(3*H*)-one (structures **1**, **4**, **5-7** in Fig. 1). The potency and selectivity of these compounds supports their suitability as templates for the design of new BChE-selective inhibitors and/or fluorogenic ligands which could be used as probes in diverse biological applications.

2. Materials and methods

2.1. Synthesis

2.1.1. Materials and general procedures

Melting points were determined in a capillary tube and are uncorrected. IR spectra were recorded on Specord IR-75 spectrometer or on Infracum FT-801 Fourier spectrometer in KBr pellets (for the crystalline

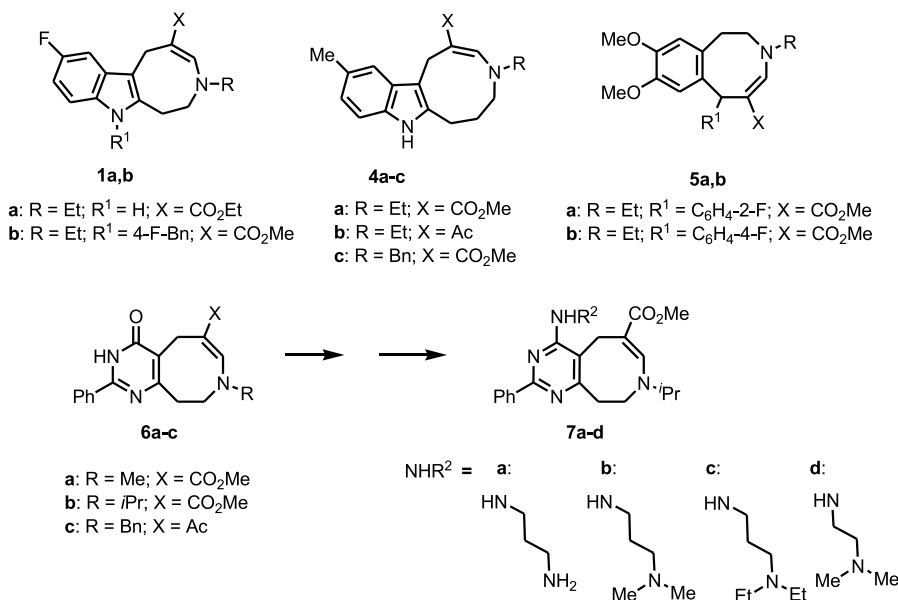
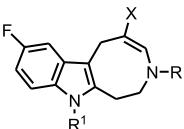
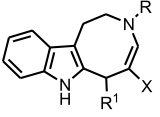
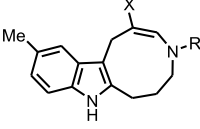
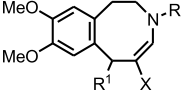
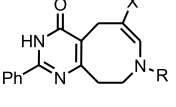
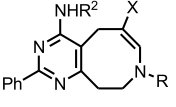
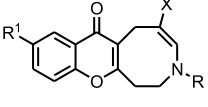


Fig. 1. Structures of partially saturated annelated azocine (**1**, **5-7**) and azonine (**4**) derivatives.

Table 1
Inhibitory potency (IC₅₀, μM) on cholinesterases (AChE and BChE)^a and lipophilicity parameters of partially saturated annelated azocine and azonine derivatives.

Cmpd	X	R	R ¹	R ²	eeAChE	hAChE	eqBChE	hBChE	cLog P ^c	log k _w ^d
										
1a ^b	CO ₂ Et	Et	H	–	8.40 ± 1.10		≈100		4.02	4.50
1b ^b	CO ₂ Me	Et	4'-F-Bn	–	15.1 ± 1.40		≈40		5.64	5.72
										
3a	CO ₂ Me	Et	2'-F-Ph	–	9.70 ± 0.50		>20		4.92	4.85
3b	CO ₂ Me	Et	2'-F-6'-Cl-Ph	–	5.23 ± 1.30		>20		5.08	5.50
3c	CO ₂ Me	4'-F-Bn	ⁱ Pr	–	8.20 ± 0.92		5.50 ± 1.06		6.09	6.27
3d	CO ₂ Me	4'-F-Bn	Bn	–	8.82 ± 1.12		8.84 ± 0.78		6.83	6.53
3e	Ac	4'-F-Bn	Bn	–	1.89 ± 0.31	6.68 ± 1.04	>20	0.340 ± 0.008	6.83	6.58
										
4a	CO ₂ Me	Et	–	–	19.1 ± 1.0		>20		4.31	4.47
4b	Ac	Et	–	–	1.79 ± 0.40	8.68 ± 0.86	>20	8.41 ± 0.45	4.31	3.88
4c	CO ₂ Me	Bn	–	–	9.63 ± 0.85	10.7 ± 1.2	6.60 ± 0.20	2.47 ± 0.04	5.61	5.36
										
5a	CO ₂ Me	Et	2'-F-Ph	–	9.59 ± 0.70		>20		4.74	4.30
5b	CO ₂ Me	Et	4'-F-Ph	–	26.8 ± 1.90		>20		4.74	4.45
										
6a	CO ₂ Me	Me	–	–	28.8 ± 2.4		33.2 ± 1.8		2.01	2.84
6b	CO ₂ Me	ⁱ Pr	–	–	>20	12.9 ± 1.0	1.30 ± 0.92	23.7 ± 4.1	2.89	3.11
6c	Ac	Bn	–	–	7.66 ± 0.97	10.7 ± 1.1	1.90 ± 0.95	11.1 ± 0.7	3.85	3.96
										
7a	CO ₂ Me	ⁱ Pr	–	(CH ₂) ₃ NH ₂	18.4 ± 1.2	4.80 ± 0.07	0.930 ± 0.020	2.08 ± 0.08	2.69	3.02
7b	CO ₂ Me	ⁱ Pr	–	(CH ₂) ₃ NMe ₂	>20		0.421 ± 0.022		3.42	3.08
7c	CO ₂ Me	ⁱ Pr	–	(CH ₂) ₃ NEt ₂	>20	26.9 ± 0.07	0.105 ± 0.018	0.0023 ± 0.0011	4.48	3.30
7d	CO ₂ Me	ⁱ Pr	–	(CH ₂) ₂ NMe ₂	>20		0.351 ± 0.034		3.09	2.99
										
10a	CO ₂ Me	Bn	H	–		18.9 ± 3.4		23.5 ± 0.5	4.80	4.78
10b	CO ₂ Me	Bn	Br	–		20.8 ± 1.0		>20	5.77	5.70
Donepezil					0.0232 ± 0.002	0.0173 ± 0.002	2.68 ± 0.22	4.80 ± 1.00		
Tacrine					0.307 ± 0.02	0.0932 ± 0.005	0.025 ± 0.002	0.0242 ± 0.001		

^a Mean IC₅₀ (μM) ± SD, n = 3; >20 for compounds showing less than 30 % inhibition at the maximum inhibitor concentration tested, that is 20 μM; *ee*: electric eel; *eq*: equine serum; *h*: human.

^b Tested in previous work [6].

^c Calculated log P with ACDLabs software release 10.0 (Advanced Chemistry Development, Inc., Toronto, Canada).

^d Lipophilicity expressed as log of RP-HPLC polycratic capacity factor ($\log k'_{w}$, see Materials and Methods section).

substances) or as neat samples (for oils). Only noteworthy IR absorptions [cm^{-1}] are listed. ^1H and ^{13}C NMR spectra were recorded in $\text{DMSO}-d_6$ solution at 40°C or in CDCl_3 solution at 25°C on a Bruker DPX-300 (300 and 75 MHz, respectively) or on a Bruker WHT 400 instrument (400 and 100 MHz for ^1H and ^{13}C , respectively) or on an Agilent Spectrometer Technologies (500 MHz for ^1H ; 126 MHz for ^{13}C) using the residual signal of nondeuterated solvent as the internal standard. The chemical shift data are expressed in parts per million (δ) and the coupling constants J are in hertz (Hz); the following abbreviations are used for multiplicity: s, singlet; d, doublet; dd, doublet-doublet; td, triplet of doublets; t, triplet; q, quartet; m, multiplet. Mass spectra were obtained by the ESI method (Agilent 1100 Series LC/MSD Trap System VL, electrospray ionization) or the EI technique (Finnigan-MAT 95 XL Engine, EI, 70 eV). Silufol UV-254 and Sorbfil PTLIC-AF-A-UF plates were used for TLC (visualization with UV light at 254 nm or iodine vapor). Silica gel from Acros Organics (grain size 0.04–0.06 mm, 60 Å) was used for column chromatography. All the solvents were distilled before use. Methyl propiolate, acetylacetylene, trifluoromethanesulfonic anhydride and corresponding primary or secondary amines (Acros Organics) were used without further purification.

The ^1H and ^{13}C NMR spectra of the newly synthesized compounds **3a-e**, **10a** and **10b**, and three representative previously reported compounds, namely **6b**, **6c** and **7c**, are reported in the Supplementary Material (Figs. S1–S10).

2.1.2. General procedure for synthesis of annulated azocines and azonines

The synthetic procedures of the herein investigated derivatives of 2,3,6,11-tetrahydro-1H-azocino[4,5-b]indole (**1a**, **b**) [6], 1,4,5,6,7,8-hexahydroazocino[5,6-b]indole (**4a-c**) [20,21], 8,9-dimethoxy-1,2,3,6-tetrahydro-3-benzoazocine (**5a**, **b**) [22,23], 4-oxo-2-phenyl-3,4,5,8,9,10-hexahydropyrimido[4,5-d]azocine (**6a-c**) [24,25] and related 4-aminoalkylamino derivatives from **6b** (**7a-d**) [26], were described in previous works. Using similar procedures 2,3,6,7-tetrahydro-1H-azocino[5,4-b]indole derivatives (**3a-e**) and 7-oxo-1,3,6,7-tetrahydro-2H-chromeno[2,3-d]azocine derivatives (**10a**, **b**) were synthesized in this study.

2.1.2.1. Synthesis of 2,3,6,7-tetrahydro-1H-azocino[5,4-b]indole derivatives (**3a-e**)

Methyl propiolate (1.2 mmol) or acetyl acetylene (1.2 mmol) was added to the solution of condensed tetrahydropyridines **2a-e** in MeCN (10 mL). The reaction of compounds **2a**, **b** was carried out at room temperature from 2 h to 42 h, and the reaction mixture for β -carboline **2c-e** was refluxed with electron deficient alkynes for 6–10 days. In the case of 1- R^1 -N-benzyl-substituted β -carboline (**2c-e**), the reactions required excesses of the alkynes (5–8 mmol) to proceed. The reaction progress was controlled by TLC (1:2 EtOAc–hexane). After completion of reaction the solvent was evaporated under reduced pressure and the crude mixture was purified by flash column chromatography on SiO_2 using EtOAc and hexane as eluent to give fused azocines **3a-e**.

Methyl (4E)-3-ethyl-6-(2-fluorophenyl)-2,3,6,7-tetrahydro-1H-azocino [5,4-b] indole-5-carboxylate (3a): Yield: 75% (in MeCN), 56% (in MeOH); beige solid; m.p. 198–199°C. IR spectrum, ν (KBr): 1649 (C=O), 3279 (N–H) cm^{-1} . ^1H NMR (600 MHz, $\text{DMSO}-d_6$): δ 11.07 (s, 1H; N–H), 7.72 (s, 1H; 4–CH), 7.41 (d, $J = 7.6$ Hz, 1H; CH–Ar), 7.34–7.31 (m, 1H; CH–Ar), 7.28 (d, $J = 7.6$ Hz, 1H; CH–Ar), 7.06 (t, $J = 7.6$ Hz, 1H; CH–Ar), 7.01–6.96 (m, 2H; CH–Ar), 6.82 (d, $J = 8.1$ Hz, 1H; CH–Ar), 6.68–6.66 (m, 1H; CH–Ar), 5.91 (s, 1H; 6–CH), 3.65 (s, 3H; O–CH₃), 3.41–3.37 (m, 1H; 2–CH₂), 3.28–3.21 (m, 2H; CH₂–CH₃), 3.15–3.07 (m, 2H; 2–CH₂, 1–CH₂), 2.65–2.62 (m, 1H; 1–CH₂), 1.05 (t, $J = 7.1$ Hz, 3H; CH₂–CH₃). ^{13}C NMR (151 MHz, $\text{DMSO}-d_6$): δ 169.8, 162.4 (d, $J = 244.2$ Hz, 1C), 150.8, 150.0 (d, $J = 5.8$ Hz, 1C), 135.9,

134.5, 130.5 (d, $J = 8.7$ Hz, 1C), 129.1, 121.9, 120.7, 118.2, 117.7, 112.5 (d, $J = 8.7$ Hz, 1C), 112.3 (d, $J = 7.2$ Hz, 1C), 110.7, 106.7, 94.0, 51.00, 50.95, 46.3, 40.4, 25.6, 14.7. LC-MS m/z : 379 [$M+H$]⁺; Anal. calcd. for $\text{C}_{23}\text{H}_{23}\text{N}_2\text{O}_2\text{F}$: C, 73.00; H, 6.13; N, 7.40. Found: C, 73.13, H, 6.15, N, 7.42.

Methyl (4E)-6-(2-chloro-6-fluorophenyl)-3-ethyl-2,3,6,7-tetrahydro-1H-azocino [5,4-b] indole-5-carboxylate (3b): Yield: 63% (in MeCN); beige solid; m.p. 210–211°C. ^1H NMR (500 MHz, CDCl_3): δ 8.07 (s, 1H, N–H), 7.56 (s, 1H, 4–CH), 7.40 (d, $J = 7.8$ Hz, 1H, CH–Ar), 7.30 (d, $J = 8.0$ Hz, 1H, CH–Ar), 7.19–7.02 (m, 4H, CH–Ar), 6.93–6.90 (m, 1H, CH–Ar), 5.98 (s, 1H, 6–CH), 4.07–4.04 (m, 1H, 2–CH₂), 3.71 (s, 3H, O–CH₃), 3.31–3.08 (m, 4H, CH₂–CH₃, 1–CH₂), 2.69–2.67 (m, 1H, 2–CH₂), 1.13 (t, $J = 7.2$ Hz, 3H, CH₂–CH₃). ^{13}C NMR (126 MHz, CDCl_3): δ 170.2, 161.6 (d, $J = 250.4$ Hz, 1C), 151.5, 136.0, 135.3, 134.4, 130.1 (d, $J = 8.5$ Hz, 1C), 129.5, 127.9 (d, $J = 10.6$ Hz, 1C), 127.0 (d, $J = 3.4$ Hz, 1C), 121.5, 119.0, 117.9, 115.7 (d, $J = 25.2$ Hz, 1C), 110.6, 107.8, 95.5, 51.8, 51.4, 47.5, 39.3, 25.4, 15.1. LC-MS m/z : 415 [$M(^{37}\text{Cl}) + H$]⁺, 413 [$M(^{35}\text{Cl}) + H$]⁺. Anal. calcd. for $\text{C}_{23}\text{H}_{22}\text{N}_2\text{O}_2\text{FCl}$: C, 66.91; H, 5.37; N, 6.78. Found: C, 66.93; H, 5.37; N, 6.82.

Methyl (4E)-3-(4-fluorobenzyl)-6-(propan-2-yl)-2,3,6,7-tetrahydro-1H-azocino [5,4-b] indole-5-carboxylate (3c): Yield: 30% (in MeCN); colorless solid; m.p. 187–189°C. IR spectrum, ν (KBr): 1655 (C=O), 3300 (N–H) cm^{-1} . ^1H NMR (300 MHz, CDCl_3): δ 7.96 (s, 1H; N–H), 7.76 (s, 1H; 4–CH), 7.27–7.00 (m, 6H; CH–Ar), 6.84 (t, $J = 8.4$ Hz, 2H; CH–Ar), 4.41 (d, $J = 15.4$ Hz, 1H; CH₂–Ar), 4.34 (d, $J = 15.4$ Hz, 1H; CH₂–Ar), 4.14 (d, $J = 10.3$ Hz, 1H; 6–CH), 4.11–4.06 (m, 1H; 2–CH₂), 3.70 (s, 3H; O–CH₃), 3.41 (ddd, $J = 2.2, 4.3, 14.8$ Hz, 1H; 2–CH₂), 2.99–2.79 (m, 2H; 1–CH₂), 2.10–2.00 (m, 1H; CH₃–CH–CH₃), 1.06 (d, $J = 6.3$ Hz, 3H; CH₃–CH–CH₃), 0.92 (d, $J = 6.3$ Hz, 3H; CH₃–CH–CH₃). ^{13}C NMR (75 MHz, CDCl_3): δ 171.4, 162.4 (d, $J = 246.7$ Hz, 1C), 152.2, 137.5, 134.2, 133.2 (d, $J = 2.9$ Hz, 1C), 129.9, 128.9 (d, $J = 8.0$ Hz, 2C), 121.1, 118.9, 117.6, 115.6 (d, $J = 21.8$ Hz, 2C), 110.3, 107.0, 97.8, 60.9, 51.4, 49.5, 45.5, 38.9, 25.5, 22.7, 20.4. LC-MS m/z : 407 [$M+H$]⁺. Anal. calcd. for $\text{C}_{25}\text{H}_{27}\text{FN}_2\text{O}_2$: C, 73.87; H, 6.69; N, 6.89. Found: C, 73.85; H, 6.70; N, 6.88.

Methyl (4E)-6-benzyl-3-(4-fluorobenzyl)-2,3,6,7-tetrahydro-1H-azocino [5,4-b] indole-5-carboxylate (3d): Yield: 38% (in MeCN); colorless solid; m.p. 190–192°C; IR spectrum, ν (KBr): 1650 (C=O), 3296 (N–H) cm^{-1} . ^1H NMR (300 MHz, CDCl_3): δ 7.78 (s, 1H; N–H), 7.74 (s, 1H; 4–CH), 7.27–7.25 (m, 1H; CH–Ar), 7.17–7.01 (m, 10H; CH–Ar), 6.84 (t, $J = 8.6$ Hz, 2H; CH–Ar), 4.71 (dd, $J = 3.5, 10.1$ Hz, 1H; 6–CH), 4.45 (d, $J = 15.4$ Hz, 1H; CH₂–Ar), 4.33 (d, $J = 15.4$ Hz, 1H; CH₂–Ar), 4.29–4.18 (m, 1H; 2–CH₂), 3.66 (s, 3H; O–CH₃), 3.64–3.56 (m, 1H; 2–CH₂), 3.25 (dd, $J = 3.7, 12.8$ Hz, 1H; 1–CH₂), 3.17–2.99 (m, 3H; 1–CH₂, CH₂–Ph). ^{13}C NMR (75 MHz, CDCl_3): δ 170.5, 162.4 (d, $J = 246.1$ Hz, 1C), 152.6, 135.6, 134.3, 133.1 (d, $J = 3.4$ Hz, 1C), 129.8, 128.9 (d, $J = 7.5$ Hz, 2C), 128.8 (2C), 128.2 (2C), 126.0 (2C), 121.2, 118.8, 117.6, 115.6 (d, $J = 21.2$ Hz, 2C), 110.4, 107.9, 99.1, 60.6, 51.4, 50.6, 47.5, 41.7, 25.4. LC-MS m/z : 455 [$M+H$]⁺. Anal. calcd. for $\text{C}_{29}\text{H}_{27}\text{FN}_2\text{O}_2$: C, 76.63; H, 5.99; N, 6.16. Found: C, 76.65; H, 5.98; N, 6.17.

1-[(4E)-6-benzyl-3-(4-fluorobenzyl)-2,3,6,7-tetrahydro-1H-azocino [5,4-b] indol-5-yl] ethanone (3e): Yield: 25% (in MeCN); colorless solid; m.p. 217–219°C; IR spectrum, ν (KBr): 1614 (C=O), 3222 (N–H) cm^{-1} . ^1H NMR (500 MHz, CDCl_3): δ 7.54 (s, 1H, N–H), 7.41 (s, 1H, 4–CH), 7.26–7.25 (m, 2H, CH–Ar), 7.18–6.99 (m, 9H, CH–Ar), 6.88 (t, $J = 8.5$ Hz, 2H, CH–Ar), 4.91 (dd, $J = 3.6, 10.5$ Hz, 1H, 6–CH), 4.49 (d, $J = 15.4$ Hz, 1H, CH₂–Ar), 4.39 (d, $J = 15.4$ Hz, 1H, CH₂–Ar), 4.33–4.27 (m, 1H, 2–CH₂), 3.64–3.61 (m, 1H, 2–CH₂), 3.17–3.02 (m, 4H, 1–CH₂, CH₂–Ph), 2.24 (s, 3H, CO–CH₃). ^{13}C NMR (126 MHz, CDCl_3): δ 195.0, 162.4 (d, $J = 246.7$ Hz, 1C), 154.5, 140.9, 135.7, 134.2, 132.5 (d, $J = 3.2$ Hz, 1C), 129.7, 128.9 (d, $J = 7.2$ Hz, 2C), 128.2 (2C), 126.0 (2C), 121.1, 118.8, 117.5, 115.8 (d, $J = 21.6$ Hz, 2C), 113.4, 110.4, 110.0, 107.8, 60.7, 50.6, 47.0, 39.6, 25.5, 25.3. LC-MS m/z : 439 [$M+H$]⁺. Anal.

calcd. for $C_{29}H_{27}FN_2O$: C, 79.43; H, 6.21; N, 6.39. Found: C, 79.44; H, 6.20; N, 6.40.

2.1.2.2. Synthesis of 7-oxo-1,3,6,7-tetrahydro-2H-chromeno[2,3-d]azocine derivatives (10a,b). Methyl propiolate (1.2 mmol, 1.2 equiv) was added to the solution of compound **8a** or **8b** (1.0 mmol, 1 equiv) in trifluoroethanol (5 mL) cooled to $-16\text{ }^{\circ}\text{C}$. The reaction mixture was kept at $-16\text{ }^{\circ}\text{C}$ for 3 days and the reaction progress was controlled by TLC (eluent 1:1 EtOAc–hexane). The solvent was evaporated under reduced pressure, and the reaction mixture was separated using column chromatography to isolate compounds **9** and **10** (silica gel, EtOAc–hexane, 1:3). Compound **9** was synthesized and characterized earlier [51], whereas **10** was prepared for the first time.

Methyl (4E)-3-benzyl-7-oxo-1,3,6,7-tetrahydro-2H-chromeno[2,3-d]azocine-5-carboxylate (10a): Yield 32 %; colourless crystals; m.p. $160\text{--}161\text{ }^{\circ}\text{C}$. IR spectrum, ν (KBr): 1685 (C=O), 1637 (C=O) cm^{-1} . ^1H NMR (600 MHz, CDCl_3) δ : 8.19–8.16 (m, 1H, H-8), 7.61 (s, 1H, NCH), 7.57(ddd, $J = 8.7, 7.0, 1.6$ Hz, 1H, H-11), 7.32 (m, 1H, H-9), 7.23–7.19 (m, 2H, Bn), 7.17–7.14 (m, 2H, H-10, Bn), 7.02 (d, $J = 7.43$ Hz, 2H, Bn), 4.33 (s, 2H, 6- CH_2), 3.99 (s, 2H, CH_2 -Bn), 3.82 (t, $J = 6.61$ Hz, 2H, 2- CH_2), 3.76 (s, 3H, CO_2CH_3), 2.97 (t, $J = 6.61$ Hz, 2H, 1- CH_2). ^{13}C NMR (151 MHz, CDCl_3) δ : 177.4, 169.9, 163.7, 152.0, 147.7, 146.5, 137.4, 128.8 (2C), 127.9, 127.4, 124.1, 123.9, 120.0, 117.1, 114.7, 114.8, 96.9, 61.3, 51.5, 47.8, 35.8, 18.5. LC-MS, m/z : 376 $[\text{M}+\text{H}]^+$. HRMS (MALDI +) m/z calcd for $\text{C}_{23}\text{H}_{21}\text{NO}_4$ in form of $[\text{M}+\text{H}]^+$ ion 376.1543, found: 376.1521.

Methyl (4E)-3-benzyl-9-bromo-7-oxo-1,3,6,7-tetrahydro-2H-chromeno[2,3-d]azocine-5-carboxylate (10b). Yield 28 %; light yellow crystals; m.p. $204\text{--}206\text{ }^{\circ}\text{C}$. IR spectrum, ν (KBr): 1665 (C=O), 1627 (C=O) cm^{-1} . ^1H NMR (600 MHz, CDCl_3) δ : 8.28 (d, $J = 2.5$ Hz, 1H, H-8), 7.64 (dd $J = 8.7, 2.5$ Hz, 1H, H-11), 7.60 (s, 1H, NCH), 7.20 (m, 1H, H-10), 7.16 (t, $J = 7.6$ Hz, 2H, Bn), 7.09–7.07 (m, 3H, Bn), 4.32 (s, 2H, 6- CH_2), 3.97 (s, 2H, CH_2 -Bn), 3.81 (t, $J = 6.4$ Hz, 2H, 2- CH_2), 3.75 (s, 3H, CO_2CH_3), 2.95 (t, $J = 6.6$ Hz, 2H, 1- CH_2). ^{13}C NMR (151 MHz, CDCl_3) δ : 176.06, 169.74, 164.13, 154.51, 151.92, 137.52, 135.92, 128.89, 128.82, 128.07, 127.53 (2C), 124.12, 120.28, 119.64 (2C), 117.77, 96.76, 61.69, 51.50, 48.04, 35.85, 18.56. LC-MS, m/z : 454 $[\text{M}+\text{H}]^+$. HRMS (MALDI +) m/z calcd for $\text{C}_{23}\text{H}_{20}\text{BrNO}_4$ in form of $[\text{M}+\text{H}]^+$ ion 454.0648, found: 454.0659.

2.2. Physicochemical profiling

2.2.1. Potentiometric determination of pK_a and $\log P$

The experimental potentiometric determinations of acidity (pK_a) and partition coefficient ($\log P$) were performed on Sirius GLpKa (Sirius Analytical Instruments Ltd., Forest Row, East Sussex, UK) computerized titration instrument, according to a procedure already described [6,27]. All experiments were carried out under a slow argon flow to avoid absorption of CO_2 at high pHs.

To determine the aqueous pK_a values, a right amount of each compound was dissolved in 20 mL of water adjusted for ionic strength (0.15 M KCl), to achieve final sample concentration in the range $5 \times 10^{-4}\text{--}1 \times 10^{-3}$ M. All titrations were recorded in the pH range 1.8–12.2 at $25 \pm 0.5\text{ }^{\circ}\text{C}$, by using standardized 0.5 M HCl or 0.5 M carbonate-free KOH as titrating agents, prepared by diluting one ampule of volumetric concentrate HCl and KOH in 1 L of fresh bidistilled water. The maximum titrant volume increment for one titration step was limited to 0.25 mL, and the pH change per titrant addition limited to 0.2 pH units. The pH value in each point was accepted when the pH-drift was lower than 0.002 pH per minute. Direction of titrations (called “up assay” and “down assay” from low to high or from high to low pH, respectively) was chosen based on the aqueous solubility of the test compound.

Evaluation of the pH-electrode efficiency was every day achieved by measurement of a blank titration and determination of Four-Plus™ parameters in Orion pH 7.00 buffer by the Bjerrum plots. For compounds

with low aqueous solubility, methanol was added as the cosolvent; the aqueous pK_a values were estimated from at least three measurements carried out in water/methanol mixtures by adding cosolvent (ranging from 60 to 20 %) and extrapolating the value by Yasuda-Shedlowsky plot (obs $pK_a + \log[\text{H}_2\text{O}]$ against inverse of the dielectric constant of mixture) [28].

The $\log P$ values were tentatively determined for some compounds by potentiometric titrations carried out in a biphasic system constituted by 0.15 M KCl and added water-saturated *n*-octanol, as apolar solvent. Titration curves were recorded in the presence of different volumes of organic solvent (at least three different solvent:water, v/v, ratios ranging from 0.1 to 10) and the results plotted against logarithm of phase ratio. All data were processed by using RefinementPro software (Sirius Analytical Instruments Ltd., Forest Row, East Sussex, UK).

2.2.2. Determination of lipophilicity by RP-HPLC

Lipophilicity of the whole series of compounds was determined by RP-HPLC according to methods previously reported [9,29]. Capacity factors ($\log k'$) were measured using a Phenomenex (Phenomenex Italy, Castel Maggiore, Italy) Kinetex C18 column (150×4.6 mm i.d., $5\text{ }\mu\text{m}$ particles) as the non-polar stationary phase, at regular increments of the volume fraction of methanol (φ) in the aqueous mobile phase (0.01 M ammonium formate buffer, pH 5.0). All the measurements were made at $25 \pm 1\text{ }^{\circ}\text{C}$, the flowrate set at 1.0 mL/min, and detection at 254 nm on Agilent 1200 Series LC System, equipped with DAD detector (Agilent Technologies). Capacity factors (k') of each compound at different mobile phase compositions (0.05-increments of methanol φ) were calculated as: $k' = (t_R - t_0)/t_0$, where t_R is the retention time of the solute and t_0 is the column dead time, measured as the solvent front. The $\log k'$ values increased linearly ($r^2 > 0.95$) with decreasing methanol volume fraction (φ). Finally, the $\log k'_w$ at $\varphi = 0$ was calculated using Eq. (1):

$$\log k' = \log k'_w - S\varphi \quad (1)$$

where S (slope) is a constant for the solute–eluent combination.

2.2.3. Determination of aqueous solubility

Aqueous solubility was measured for some selected compounds under kinetic solubility conditions in aqueous buffer solution (50 mM PBS, pH 7.4, 0.15 M KCl) at $37\text{ }^{\circ}\text{C}$ by U-HPLC, according to previously described protocols [7,30].

For each compound, a 10 mM stock solution in DMSO was solubilized in PBS (50 mM) to obtain a final concentration of 200 μM . After shaking of the suspension in an orbital shaker for 2 h at 250 rpm, the solution was separated by centrifugation (2500 rpm, 3 min) and filtered. An equal volume of solution was transferred into 1:1 (v/v) mixture of DMSO/PBS. The concentration of compound was determined by U-HPLC and UV detector (254 nm) by comparing the peak area of external standard solution. All data were mean of at least three independent experiments. Analytical chromatographic conditions: mobile phase, MeOH/ammonium formate 10 mM pH 4.5 (at various composition); column: Kinetex C18, 150×2.1 mm, $2.6\text{ }\mu\text{m}$; flow: 0.3 mL/min; injection: 2 μL . HPLC analyses were performed on an Agilent U-HPLC 1260 Infinity Quaternary LC system (Agilent Technologies, Milan, Italy).

2.3. Biological activity studies

2.3.1. Inhibition assays of cholinesterases

Electric eel AChE (eeAChE), human recombinant AChE (hAChE), equine BChE (eqBChE) and BChE from human serum (hBChE) were purchased from Sigma Aldrich (Milan, Italy). The experiments were performed in 96-well plates (Greiner Bio-One, Kremsmünster, Austria) on the Infinite M1000 Pro plate reader (Tecan, Cernusco s.N., Italy).

The inhibition of AChE or BChE was determined by applying the Ellman's spectrophotometric method, as described in previously reported protocols [31,32]. The AChE activity was determined in an assay

solution containing AChE (0.09 U/mL), 5,5-dithiobis(2-nitrobenzoic acid) (i.e., the Ellman's reagent, 0.33 mM), the test compound (20 μ M concentration, or seven scalar concentrations for compounds achieving >30 % enzyme inhibition at 20 μ M), in 0.1 M PBS pH 8.0. After 20 min incubation at 25 °C, acetylthiocholine iodide (ATC, 0.5 mM) was added, and its hydrolysis rate was monitored for 5.0 min at 412 nm. The BChE inhibitory activity was similarly determined by using BChE (0.2 U/mL) and butyrylthiocholine iodide (0.5 mM) as the substrate. The results were reported as the IC₅₀ values, determined by the nonlinear regression method 'log[inhibitor] vs. response', expressed as the mean \pm SD of at least three independent measurements, each one performed in duplicate. The curve fitting for determination of the IC₅₀ values was calculated by nonlinear regression, using Prism software (version 5.01 for Windows; GraphPad Software, San Diego, CA, USA).

2.3.2. Inhibition assay of monoamine oxidase

The isoforms A and B of human recombinant monoamine oxidase (MAO) from baculovirus-infected insect cells used for inhibition assays were purchased from Sigma Aldrich (Milan, Italy). Experiments were performed in 96-well plates (Greiner Bio-One, Kremsmünster, Austria) on the Infinite M1000 Pro plate reader (Tecan, Cernusco s.N., Italy).

In the MAO inhibition assays [33], the test compounds, at 10 μ M concentration, were preincubated for 20 min at 37 °C with 50 μ M kynuramine as the substrate in 0.1 M phosphate buffer solution (PBS) pH 8.0 made 0.39 osmolar with KCl. After the addition of human recombinant hMAO A (250 U/mg) or hMAO B (59 U/mg) and further 30 min incubation, NaOH was added, and the developed fluorescence read at 310/400 nm excitation/emission wavelength. For compounds achieving at least 50 % inhibition at 10 μ M concentration, seven scalar concentrations of each inhibitor were tested and the concentration achieving 50 % inhibition of the MAO activity (IC₅₀) was calculated by nonlinear regression, using Prism software. Inhibition data were expressed as mean \pm SD of three independent measurements, each one performed in duplicate.

2.3.3. P-glycoprotein inhibition assay

Compounds were screened as inhibitors of P-glycoprotein (P-gp) using the fluorescence calcein-AM assays in MDCK cell lines overexpressing P-gp. The experiments were conducted according to the reported procedure [30]. The transfected MDCK cell line (50000 cells per well) was seeded in a black Culture-Plate 96-well plate with medium (100 μ L) and allowed to become confluent overnight. The test compounds (100 μ L), at concentrations ranging from 0.1 to 100 μ M, were solubilized in culture medium and added to each well. The 96-well plate was incubated 30 min at 37 °C. Calcein-AM in PBS (100 μ L) was added to each well to a final concentration of 2.5 μ M, and the plate was incubated for additional 30 min. The plate was washed 3 times with ice-cold PBS (100 μ L). Saline buffer (100 μ L) was added to each well, and the plate was read with a Victor3 spectrofluorimeter (PerkinElmer) at excitation and emission wavelengths of 485 and 535 nm, respectively. Under these conditions, calcein cell accumulation in the absence and presence of the test compounds was evaluated and the fluorescence basal level was estimated in the untreated cells. The increase of fluorescence intensity in treated cells over the basal level was measured. IC₅₀ values were determined by fitting the fluorescence increase percentage against log [concentration] of the inhibitor.

2.3.4. Cytotoxicity assay on HepG2 cell line

The antiproliferative assay was performed in HepG2 cells at 48 h [30]. On the first day, 10000 cells per well were seeded in 96-well plates in a volume of 100 μ L. On the second day, the test compounds, each at concentrations ranging from 0.1 to 100 μ M, were added. In all experiments, DMSO were added in each control to evaluate a possible solvent cytotoxicity. After the incubation time with test compounds (48 h), MTT (0.5 mg/mL) was added to each well, and after 3 h incubation (at 37 °C), the supernatant was removed. The formazan crystals were solubilized

with DMSO (100 μ L), and the absorbance values at 570 and 630 nm were measured with the microplate reader Victor3.

2.4. In-silico studies

To understand the binding mode of compounds **7a** and **7c** to eqBChE and hBChE, whose inhibition potency data differ greatly (see below), a computational protocol that included modeling of the 3D structure of eqBChE, docking, Molecular Dynamics (MD) and binding free energies calculations was used.

2.4.1. Modeling of equine serum BChE

Among the X-ray structures of hBChE available in the Protein Data Bank, 1P0M [34] and 6QAA [35] were chosen to explore the binding mode of **7a** and **7c**. The choice of these structures was motivated by the absence of covalent linkages with compounds present in the binding site, which might introduce alterations affecting the docking of **7a** and **7c**, the resolution factor of these X-ray structures (resolution of 2.4 and 1.9 Å, respectively), and the structural variability of certain residues, such as Gln71 and Tyr237, which might influence the proper accommodation of the ligands, especially at the outer region of the binding pocket.

Due to the lack of 3D structures of eqBChE, a homology model was built using both 1P0M and 6QAA as templates. This approach takes advantage of the high sequence identity (~90 %) [36] between human and equine enzymes. The 3D models were generated using SWISSMODEL [37], leading to structures named EQ (1) and EQ (2) (see Supplementary Material Tables S1 and S2 for details).

2.4.2. Molecular docking calculation

Docking of **7a** and **7c** was performed with Glide [38] using the XP score function. A 40/60 Å inner/outer box centered in residues present in the gorge was chosen with the aim to encompass the binding cavity, including the catalytic gorge and peripheral sites (the center of the grid is given by coordinates $x = 17.42$, $y = 38.12$ and $z = 37.12$ Å; see Supplementary Material Fig. S11). Conformer generation and screening of ligand poses were performed using the default procedure implemented in Glide. The maximum number of poses per ligand and the number of ligand poses to be used in post-docking minimization was adjusted to 100. The energy window for retention of ring conformers was adjusted to 2.5 kcal/mol, and the RMSD used to discard poses was fixed at 0.5 Å. The best pose was mainly selected according to visual inspection of the interactions with residues in the binding pocket and the docking score. Let us note that this protocol correctly predicted the binding mode of the (S)-2-(butylamino)-N-(2-cycloheptyl-ethyl)-3-(1H-indol-3-yl)propanamide in the pocket of hBChE (PDB ID 6QAA). The best ranked poses mainly exhibited differences in the spatial arrangement of the alkylated amine, but the core of the compound overlapped well with the X-ray pose (see Supplementary Material Fig. S12). Thus, the root-mean square deviation between the X-ray ligand and the docked ligand was lower than 2 Å for the first five poses (see Supplementary Material Fig. S12).

2.4.3. Molecular dynamics simulation

The binding mode of **7a** and **7c** was refined by means of MD simulations using Amber20 software [39] and the ff99SB-ILDN force field [40] for the protein residues. Parametrization of **7a** and **7c** was performed with gaff2 forcefield [41]. Atomic point charges were defined using the RESP method [42] by fitting the HF/6-31G(d) electrostatic potential created around the molecule. The entire system was immersed in a TIP3P water box (approximate dimensions of $83 \times 87 \times 90$ Å³) [43], leading to simulations systems that contained around 17000 water molecules (ranging from 16211 to 17624 TIP3P waters). To maintain a proper neutrality of the system, seven chlorine ions were added to the simulation system.

The preparation of the system started with a three-step minimization protocol to gradually minimize the hydrogens, water molecules and

finally the whole system. Then, a six-step heating-equilibration process was performed, increasing the temperature from 100 to 300 K, imposing a cartesian restraint of 5 kcal/mol Å⁻² in different atoms of the ligand to avoid unexpected changes during heating. Next, using different equilibrated snapshots as starting models three different replicas of each system were started. For those bonds involving hydrogen atoms, SHAKE algorithm was used [44]. Electrostatic interactions were treated with Particle Mesh Ewald (PME) [45] and a cutoff of 10 Å was established for the nonbonded interactions. In the first five steps of production (covering 25 ns), the restraints were gradually removed. All the trajectories were extended for 200 ns (see [Supplementary Material Table S3](#) for a description of the MD simulations). A time step of 2 ps was used for saving the trajectory.

2.4.4. MM-GBSA binding free energy calculations

MMPBSA.py [46] was used to estimate the binding free energy of **7a** and **7c** bound to *eq*BChE and *h*BChE. The free energy of unbound ligand, protein and ligand-protein complex was decomposed in different terms: E_{int} , E_{elect} , E_{vdw} , $G_{\text{solv,pol}}$ and $G_{\text{solv,n-pol}}$ as expressed in Eq. (1), and the free energy of binding was estimated using Eq. (2).

$$G = E_{\text{int}} + E_{\text{elect}} + E_{\text{vdw}} + G_{\text{solv,pol}} + G_{\text{solv,n-pol}} - T \cdot \Delta S \quad (2)$$

where E_{int} , E_{elect} and E_{vdw} are the internal, electrostatic and van der Waals terms, respectively; $G_{\text{solv,pol}}$ stands for the contribution to solvation free energy using generalized Born solvation method and $G_{\text{solv,n-pol}}$ is the nonpolar contributions to solvation free energy computed from the solvent-accessible surface area (SASA). Given the structural resemblance of **7a** and **7c**, the entropic contribution ($T \cdot \Delta S$) was assumed to cancel in the comparison of the binding modes to *h*BChE and *eq*BChE in Eq. (3).

$$\Delta G_{\text{bind}} = G_{\text{complex}} - G_{\text{receptor}} - G_{\text{ligand}} \quad (3)$$

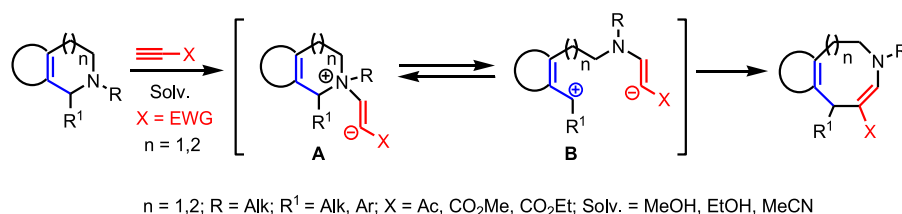
The distinct energy components were estimated using a subset of 50 snapshots collected along the last 50 ns of the trajectories.

3. Results and discussion

3.1. Chemistry

Domino reactions of annelated tetrahydropyridines and azepines with electron deficient alkynes represent an elegant and convenient method for the synthesis of condensed eight- and nine-membered azaheterocycles. This methodology for building up medium-sized azaheterocycles relies on the use tertiary cyclic amines in Michael addition reaction with alkynes ([Scheme 1](#)).

It appears crucial that the nitrogen atom must be separated by one methylene group from the annelated aromatic cycle or the double bond. The reaction is tolerant to alkyl or aryl substituents attached to methylene group. At the first stage, a nucleophilic attack of the nitrogen atom to the triple bond of the activated alkyne leads to formation of zwitterion **A**, that exists in equilibrium with the open form **B**. The interaction of two ions in the intermediate **B** completes the formation of the new ring thus increasing the cycle by two carbon atoms. Acetonitrile proved to be the preferred solvent in these reactions, but in some cases protic solvents, such as methanol and ethanol, can also be used.



Scheme 1. Domino synthesis of functionalized eight- and nine-membered azaheterocycles investigated herein as cholinesterase inhibitors.

2,3,4,9-Tetrahydro-1*H*-β-carbolines, other annelated tetrahydropyridines and 1,2,3,4,5,6-hexahydroazepino[4,3-*b*]indoles, used as starting materials for preparing azocine and azonine derivatives, had been synthesized through the Pictet-Spengler reaction or Fischer synthesis according to well-known methods [47–50]. With the aim of expanding the knowledge of structure-activity relationships (SARs) of the annelated tetrahydroazocine (and azonine as well) derivatives, some new azaheterocyclic derivatives, namely **3a-e** ([Scheme 2](#)) and **10a-b** ([Scheme 3](#)), were synthesized and several diversely decorated analogs ([Fig. 1](#)) were extracted from previously reported molecular libraries of the group of L. G. Voskressensky.

The reaction of the starting β-carbolines **2a-e** with suitable electron deficient alkynes gave the corresponding 2,3,6,7-tetrahydro-1*H*-azocine [5,4-*b*]indole derivatives **3a-e** ([Scheme 2](#)).

2,3,6,11-Tetrahydro-1*H*-azocino[4,5-*b*]indoles (**1a,b**) [6], 1,4,5,6,7,8-hexahydroazonino[5,6-*b*]indoles (**4a-c**) [20,21], 8,9-dimethoxy-1,2,3,6-tetrahydro-3-benzoazocines (**5a,b**) [22,23], 4-oxo-2-phenyl-3,4,5,8,9,10-hexahydropyrimido[4,5-*d*]azocines (**6a-c**) [24,25] and four 4-aminoalkylamino derivatives from **6b** (**7a-d**) [26], were investigated in this study for in vitro activities and SARs ([Fig. 1](#)).

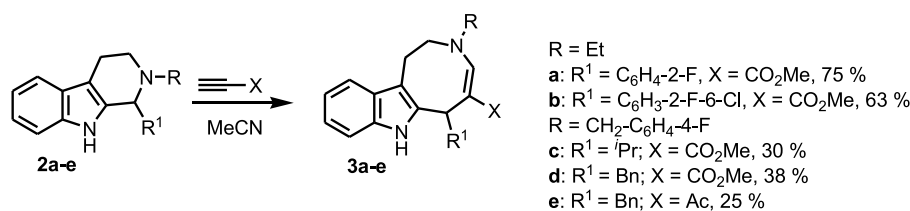
The series of annelated tetrahydroazocine β-enamino-esters was complemented with two further 7-oxo-1,3,6,7-tetrahydro-2*H*-chromeno[2,3-*d*]azocine derivatives (**10a-b**, [Scheme 3](#)). Some years ago, some of us described a convenient method for synthesizing vinyl-substituted chromones in high yields by the reactions of 1,2,3,4-tetrahydro-10*H*-chromeno[3,2-*c*]pyridin-10-ones (**8a,b**) with methylpropiolate, acetyl acetylene or dimethyl acetylenedicarboxylate in methanol at room temperature [51]. Analogous reaction carried out in trifluoroethanol as the solvent at –16°C led to the formation of 2-vinyl chromones (**9a,b**), as products of tetrahydropyridine ring cleavage, and the products of 6 → 8 ring expansion, namely the desired chromeno[2,3-*d*]azocines **10a** and **10b** in about 30 % yields.

3.2. Biological evaluation

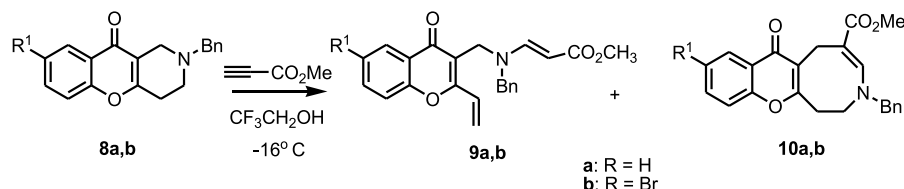
3.2.1. Inhibition of cholinesterases

To extend the knowledge of the SARs of tetrahydroazocine[4,5-*b*]indole-based β-enamino esters, like compounds **1a** and **1b**, twenty diverse previously and newly synthesized annelated tetrahydroazocine β-enamino esters or ketone derivatives were tested as potential inhibitors against AChE and BChE. For comparing the inhibition data with those previously obtained [6], all the compounds were firstly tested against *ee*AChE and *eq*BChE. The most active inhibitors, representative of the diverse tetrahydroazocine-containing subsets, were then assayed toward the human enzymes. All the compounds were tested against each isoenzyme at a single 20 μM concentration, and for those showing more than 30 % inhibition at that concentration, the IC₅₀ values were determined in at least three independent experiments ([Table 1](#)). Donepezil and tacrine were used as positive controls.

There was no correlation between the inhibition data of heterologous (*electric eel* and horse serum) and human ChEs. As for the inhibition of *ee*AChE the IC₅₀ values span a narrow range (from about 2 to just over 20 μM corresponding to **3e** and the aminoalkylamino derivatives **7a-d**, respectively), whereas in the case of *eq*BChE they span a higher range of values (from 0.1 to just over 20 μM) with an inversion of the potency



Scheme 2. Synthesis of 2,3,6,7-tetrahydro-1H-azocino[5,4-b]indole derivatives **3a-e**.



Scheme 3. Synthesis of 7-oxo-1,3,6,7-tetrahydro-2H-chromeno[2,3-d]azocine carbomethoxy ester derivatives **10a,b**.

ranking, given that **7a-d** proved to be more active than several more lipophilic compounds, including **3e**. Most of the examined compounds, regardless of the medium-sized azaheterocycle (azocine **3** vs azonine **4**), fusion isomerism (**1** vs **3**) and the annelated heterocycle, proved to be moderately potent (low micromolar range) and poorly isoform-selective, except for derivatives **7a-d**, which achieved submicromolar inhibitory potency towards *eq*BChE with a ten-to-hundred-fold selectivity over *ee*AChE. The relevance of incorporating the β -enamino ester unit into the annelated tetrahydroazocine scaffold of compounds **7** was demonstrated by the activity drop observed upon replacement of the methyl tetrahydro-1-isopropylazocine-3-carboxylate moiety in **7b** (*eq*BChE IC₅₀ = 0.42 μ M) with tetrahydro-*N*-isopropylpyridine (*eq*BChE IC₅₀ \approx 50 μ M) in the synthetic precursor of **7b**.

The inhibition data determined for the human enzymes highlight the effect of molecular lipophilicity and/or size/polarizability on the ChE inhibition potency and isoform-selectivity. The activities of **3e** and **7c** against the human isoenzymes were noteworthy in this respect. Indeed, despite the difference of more than two log *P* units, the more hydrophobic **3e** (cLog *P* = 6.83) resulted just 4-fold more active than the less hydrophobic **7c** (cLog *P* = 4.48) as *h*AChE inhibitor, whereas in contrast **7c** (IC₅₀ = 2.3 nM) was 150-fold more active than **3e** as *h*BChE inhibitor. The complete kinetics for the most potent inhibitor **7c** towards *h*BChE

showed a noncompetitive/mixed-type inhibition mechanism (Fig. 2), with inhibition constant *K*_i of 7.8 \pm 0.2 nM.

Some tetrahydroazocine-containing β -amino acetyl or COOMe ester derivatives, representative of the diversely annelated heterocyclic scaffolds, including the most potent *h*BChE inhibitors **3e** and **7c**, were assayed for their activity as MAO inhibitors, using the MAO B-selective inhibitor pargyline as the positive control. For compounds showing more than 50 % inhibition at 10 μ M, the IC₅₀ was determined in at least three independent experiments (Table 2).

Only the 9-Br congener of 7-oxo-1,3,6,7-tetrahydro-2H-chromeno[2,3-d]azocine β -enamino methyl carboxylate (**10b**) achieved single digit micromolar IC₅₀ (about 7 μ M) against MAO B, suggesting this azaheterocyclic moiety as suitable scaffold of novel MAO B-based MTDLs for neurologic disorders. All the other compounds, although weak inhibitors, showed some degree of selectivity toward MAO B.

Considering that the capacity of small organic molecules to evade or inhibit the P-gp efflux pumps may provide a preliminary assessment of their permeation into the brain crossing the blood-brain barrier [52], we found that the most active BChE inhibitors **3e**, **7a** and **7c** also inhibited P-gp with IC₅₀ values in the very low to submicromolar concentration range. In particular, the nanomolar *h*BChE inhibitor **7c** showed an IC₅₀ value of 0.27 μ M against P-gp, which would support its potential to cross the blood-brain barrier. The measurement of the cytotoxicity against the immortalized human liver cancer cell line HepG2 demonstrated that the examined molecules are weakly cytotoxic (IC₅₀ > 100 μ M) at concentrations 5–10 times higher than their IC₅₀ against ChEs. Compound **7c**, while showing a lower IC₅₀ in HepG2 (about 36 μ M), proved to be cytotoxic in HepG2 cell line at concentrations more than ten thousand

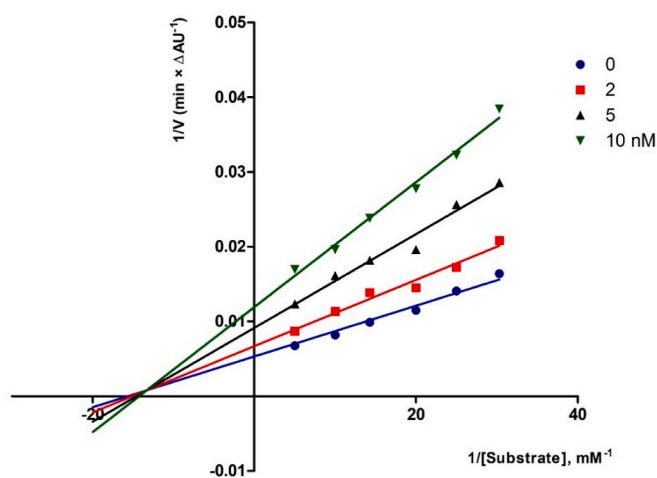


Fig. 2. Lineweaver-Burk plots of inhibition kinetics for compound **7c** toward *h*BChE; reciprocals of enzyme activity vs reciprocals of substrates' concentration in the presence of different inhibitor's concentrations (0–10 nM).

Table 2
 Inhibitory potency toward human MAO A and B, P-gp and cytotoxicity in HepG2 cell line of representative β -enamino esters of fused azocine/azonine derivatives.

Cmpd	IC ₅₀ , μ M ^a		IC ₅₀ , μ M ^{a,b}	
	<i>h</i> MAO A	<i>h</i> MAO B	P-gp	HepG2
3e	(16 \pm 4)	(44 \pm 1)	1.73 \pm 0.02	>100
4c	(26 \pm 5)	(30 \pm 4)	7.74 \pm 1.27	>100
6b	n.i.	(32 \pm 4)	46.3 \pm 10.5	>100
7a	(13 \pm 5)	(39 \pm 4)	1.64 \pm 0.40	>100
7c	(14 \pm 4)	(27 \pm 4)	0.27 \pm 0.03	35.9 \pm 2.6
10b	(29 \pm 3)	7.09 \pm 1.02	n.d.	>100
Pargyline	10.8 \pm 0.5	2.66 \pm 0.44		
Tacrine			>100	>100

^a Mean IC₅₀ (μ M) \pm SD or % inhibition \pm SD in parentheses at 10 μ M (MAOs), n = 3; n.i. = no inhibition; >100 for compounds showing less than 60 % inhibition at the maximum concentration tested (100 μ M).

times higher than the in vitro *h*BChE IC₅₀.

3.2.2. Structure-activity relationships

Relying on a more quantitative approach to SARs on ChEs' inhibitory activity and selectivity, the lipophilicity of the fused tetrahydroazocine (and hexahydroazonine) β -enamino carbomethoxy ester and acetyl derivatives was tentatively assessed by measuring their 1-octanol/water partition coefficients with both the traditional 'shake-flask' method and the potentiometric titration technique, according to protocols previously described [6,27,28]. Unfortunately, most of the examined compounds were too lipophilic ($\log P \gg 3$) to allow the apparent partition coefficients to be determined with accuracy (sometimes, precipitation at the interphase between the two immiscible conjugated solutions was visible). We therefore opted for the measurement of a relative lipophilicity scale through an RP-HPLC method [9,29]. The polycratic capacity factors ($\log k'_w$) were determined for all the compounds (Table 1). The 1-octanol–water partition coefficient (cLog P) was calculated with two computational tools (Bio-Loom software, v. 1.7 and ACDLabs software, release 9.05). The ACDLabs software was used also for calculating descriptors of polarizability and size, namely molar refractivity (*MR*) and molar volume (V_{mol}). The experimental lipophilicity RP-HPLC parameters ($\log k'_w$), along with the cLog P values, are listed in Table 1 (see also Supplementary Material Table S4).

The RP-HPLC polycratic capacity factor $\log k'_w$ resulted well linearly correlated, over a range of 4.8 log units, with cLog P from ACDLabs software ($r^2 = 0.897$; plot in Fig. 3), and not with the descriptor calculated by the Bio-Loom software ($r^2 = 0.484$), according to Eq. (4):

$$\log k'_w = 0.88 (\pm 0.07) \text{ cLog P}_{\text{ACDLabs}} + 0.49 (\pm 0.33) \quad (4)$$

$$n = 21, r^2 = 0.897, s = 0.400, F = 166.0$$

where n represents the number of data points, r^2 the coefficient of determination, and s the standard deviation of the regression equation and the F -value from the Fisher test for regression model significance (95 % confidence intervals of the regression coefficients are given in parentheses).

The slope of the regression equation (i.e., sensitivity; Eq. (4)) is close to unity (+0.9) and the intercept of about +0.5 reveals a slight, but

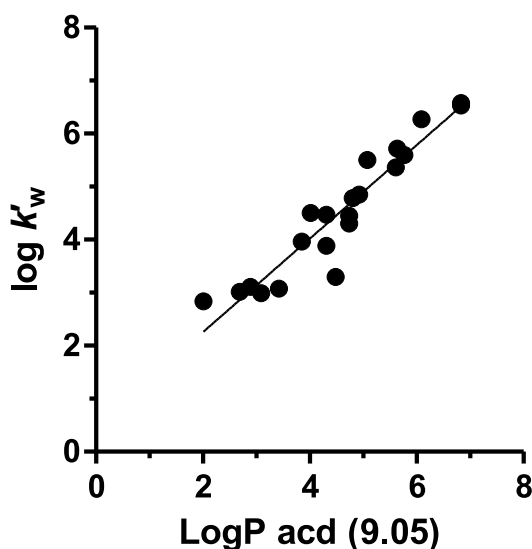


Fig. 3. Plot of correlation between experimental RP-HPLC parameter $\log k'_w$ versus $\log P$ calculated with ACDLabs software; linear regression equation (Eq. 4), $r^2 = 0.897$.

systematic positive deviation from linearity, likely due to the so-called 'silanophilic' interactions on the silica based C18 stationary phase [53, 54]. The RP-HPLC data support the suitability of cLog P values from ACDLabs expert system as predictors of lipophilicity for this series of medium-sized heterocyclic derivatives.

As can be deduced from the squared correlation matrix (Table S5), there is no noteworthy general correlation between lipophilicity parameters and inhibition data against *ee*AChE and *eq*BChE, whereas a quite good linear relationship exists between pIC_{50} (*eq*BChE) and cLog P into the subset **7a-d**.

As stated above, the inhibition potency data of recombinant human ChEs, determined for seven compounds representative of the molecular diversity in the dataset, highlight how much lipophilicity and/or size/polarizability may affect the ChEs inhibition potency and selectivity. The activities of compounds **3e** (cLog P = 6.83) and **7c** (cLog P = 4.48), which locate on the opposite ends of the explored lipophilicity scale inhibited *h*BChE with nanomolar potency, **3e** in the high nanomolar range (IC₅₀ = 340 nM) and **7c** in the very low nanomolar range (IC₅₀ = 2.3 nM). To understand this apparent inverse correlation with lipophilicity, we assessed other physicochemical properties, like acidity constants (pK_a), water solubility at pH 7.4, polarizability parameters (molar refractivity, *MR*, and molar volume, V_{mol}) using chemoinformatic and experimental tools (Table 3).

The acidity constants were measured using a reliable pH-metric technique [6,27,28]. The pK_a of the enamino nitrogen was found to fall into the range between 5.4 and 6.8 for the tetrahydroazocine derivatives **3**, **6** and **7**, basically agreeing with the values calculated by the ACDLabs software. In contrast, the experimental pK_a of enamino nitrogen in the indole-fused hexahydroazonine derivatives resulted more than one log unit higher than the predicted value, most likely due to the higher flexibility of the nine-membered azaheterocycle that could decrease the conjugation of the lone pair of the enamino nitrogen increasing its basicity in compounds **4**. The weak acidity of the NHCO/NCOH group of the 4-oxo-2-phenyl-pyrimido moiety in **6b** and **6c** or the basicity of the NR₂ basic head of the amino-alkyl chain at C4 of the pyrimidine moiety in **7a** and **7c** were consistent with those calculated by the chemoinformatic tool. For compounds **6** and **7** an additional pK_a , which was experimentally not detected most likely because too close to (or partially overlapped with) the pK_a value of the enamino function, was calculated by the ACDLabs expert system for N1 in the pyrimidone ring.

The kinetic solubility was determined for **3e**, **6b**, **6c** and **7c** in 50 mM PBS at pH 7.4 and 25 °C, and compared with the water solubility calculated at the same pH with the ACDLabs software. While **3e** was practically insoluble, according to the criteria of the US Pharmacopoeia, the *N*-(3-(diethylamino)propyl) derivative **7c**, although fortyfold less soluble than predicted by ACDLabs, due to the predominant protonated NEt₂ group at pH 7.4, can be classified as 'very soluble'. The amphoteric derivatives **6b** and **6c**, with the isoelectric points equal to 7.6 and 6.9, respectively, should exist predominantly as zwitterionic forms at pH 7.4.

Molar refractivity (*MR*) and molar volume (V_{mol}) were calculated by the ACDLabs software as parameters of bulkiness and polarizability. The lack of correlation in this molecular series between cLog P (and $\log k'_w$) and *MR* (and V_{mol}) should allow to deduce from regression models clues into the physical forces governing the binding affinity of the examined ligands to *h*BChE. The squared correlation matrix among parameters of lipophilicity and bulkiness/polarizability is reported in Table 4.

Apart from the expected high correlation between *MR* and V_{mol} ($r^2 = 0.914$) and between $\log k'_w$ and cLog P ($r^2 = 0.879$), the absence of relationship between cLog P and the polarizability parameters and the good correlation between pIC_{50} and molar volume are noteworthy for quantitative SAR (QSAR) purposes.

The best linear equation, which holds for all the seven compounds achieving finite IC₅₀ values against *h*BChE, correlates pIC_{50} with molar volume:

Table 3

Calculated and experimental physicochemical parameters of selected compounds: acidity constant (pK_a), solubility in water (S_w), molar refractivity (MR), molecular volume (V_{mol}), and the human BChE inhibitory potency (pIC_{50}).

Cmpd	$pK_a(s)^a$		$S_w, \text{mol/L}^c$		MR^d	V_{mol}^d	pIC_{50} hBChE
	calc	exp	calc	exp			
3e	6.21	6.83	$1.0 \cdot 10^{-7}$	$<1.0 \cdot 10^{-6}$	130.62	358.5	6.47
4b	7.54	8.71	$8.7 \cdot 10^{-5}$		91.06	269.3	5.08
4c	6.24	8.17	$1.4 \cdot 10^{-6}$		112.64	316.4	5.61
6b	6.29, 8.84 ^b	6.72, 8.92	$7.2 \cdot 10^{-5}$	$1.7 \pm 0.02 \cdot 10^{-4}$	99.67	287.5	4.63
6c	4.96, 8.87 ^b	6.37, 8.15	$8.6 \cdot 10^{-6}$	$1.8 \pm 0.01 \cdot 10^{-4}$	114.54	318.5	4.95
7a	5.81, 9.78 ^b	5.75, 9.44	$2.4 \cdot 10^{-2}$		118.81	351.6	5.68
7c	5.87, 10.3 ^b	5.46, 9.40	$6.8 \cdot 10^{-3}$	$1.6 \pm 0.03 \cdot 10^{-4}$	137.03	421.2	8.64

^a Acidity constant (pK_a) determined by a pH-metric technique (see Materials and Methods); values are means (RSD <5%) of three to five experiments. The lower pK_a is assigned by the program to the enamino nitrogen; the higher pK_a value is assigned to the other ionizable groups, i.e., the NHCO/NCOH group of the 4-oxo-2-phenylpyrimido moiety in **6b** and **6c** or the terminal NR_2 basic head of the amino-alkyl chain at C4 of the pyrimidine moiety in **7a** and **7c**.

^b For compounds **6** and **7** an additional pK_a (experimentally indistinguishable from the pK_a value of the enamino group) is calculated and assigned to N1 of pyrimidine ring by ACDLabs software (release 9.05, Advanced Chemistry Development, Inc., Toronto, Canada) as follows: 2.53 and 2.56 for **6b** and **6c**, respectively, and 4.45 and 4.47 for **7a** and **7c**, respectively.

^c Water solubility (mol/L) at pH 7.4 calculated by the ACDLabs software; solubility in 50 mM PBS at pH 7.4 and $25 \pm 1^\circ\text{C}$ experimentally determined according to a kinetic method as described in Materials and Methods.

^d Molar refractivity (MR , cm^3/mol) and molar volume (V_{mol} , cm^3/mol) calculated by the ACDLabs software.

Table 4

Squared correlation matrix (r^2) of the parameters of lipophilicity (cLog P, $\log k'_w$) and polarizability (MR , V_{mol}), and human BChE inhibition data ($-\log IC_{50}$) for compounds in Table 3.

	MR	V_{mol}	cLog P	$\log k'_w$	pIC_{50}
MR	1				
V_{mol}	0.914	1			
cLog P	0.156	0.050	1		
$\log k'_w$	0.073	0.001	0.879	1	
pIC_{50}	0.680	0.844	0.119	0.004	1

$$pIC_{50} (\text{hBChE}) = 2.47 (\pm 0.47) V_{mol} - 2.34 (\pm 1.59) \quad (5)$$

$$n = 7, r^2 = 0.844, s = 0.589, F = 27.13$$

A similar equation, but with lower r^2 (0.680), was obtained with molar refractivity. The inhibitory potency, pIC_{50} , appeared very poorly correlated with cLog P, but a closer inspection of the respective plot (not shown) revealed that, omitting from the regression analysis the 4-aminoalkylamino derivatives **7a** and **7c**, the other compounds fitted well the linear Eq. (6):

$$pIC_{50} (\text{hBChE}) = 0.45 (\pm 0.05) \text{cLog P}_{\text{ACDLabs}} + 3.19 (\pm 0.23) \quad (6)$$

$$n = 5, r^2 = 0.968, s = 0.148, F = 91.57$$

An equation similar for the information content to Eq. (6) was obtained by replacing cLog P with $\log k'_w$ ($r^2 = 0.979$).

The equations with positive sign of molar volume or molar refractivity in QSAR indicate that the binding of fragments of the ligand to BChE is likely affected by a combination of steric factors related to the molecular size, and the formation of van der Waals interactions with apolar residues in the binding pocket of the enzyme, which is largely shaped by hydrophobic residues. For better understanding the QSARs, we carried out an in-depth in silico study focused on the water-soluble and highly potent BChE inhibitor **7c** compared with the less active **7a**.

3.3. In-silico studies

Molecular modeling studies were performed to examine the putative binding mode of **7a** and **7c** to hBChE. Since the experimental results showed a marked difference in the IC_{50} value between recombinant human and equine serum enzymes for compound **7c** (IC_{50} values toward hBChE and eqBChE of 2.3 and 105 nM, respectively), the residue substitutions in the ligand binding site between human and equine enzymes

were examined. This analysis revealed the occurrence of five changes in the binding pocket, namely Ile69Thr, Ala277Val, Gly283Asp, Pro285Leu and Phe398Ile (Fig. 4A). In terms of structural change, Pro285Leu seems to be the most relevant one. To explore the effect of these mutations on the binding of compound **7c** to eqBChE, additional MD simulations were also performed for the complex with eqBChE and the results were compared with those obtained for the complexes with the human enzyme.

3.3.1. Molecular docking calculations

Unbiased docking calculations revealed a common pose for inhibitors **7a** and **7c** in both human and equine enzymes among the subset of best ranked poses. Inspection of the docked poses revealed that the compounds were able to adopt a similar binding mode along the gorge leading to the catalytic site in both hBChE and eqBChE (see Supplementary Material Figs. S12–S15). Thus, a common binding motif was the hydrophobic contact formed by the *N*-isopropyl unit with Trp82. This interaction was assisted by additional contacts with Trp430 (contact distances ranging from 3.2 to 4.2 Å) in the poses selected for eqBChE (EQ (1)). Furthermore, the phenyl group was located close to Trp231 (average distance of 3.5 ± 0.2 Å), with the exception of the docking pose found in hBChE (6QAA). In this pose, the arrangement of the ligand along the gorge was slightly displaced, thus reflecting the steric effect of Phe398 (replaced by Ile in eqBChE; see above), and the phenyl ring formed hydrophobic interactions with Gly117, Gln119, Ser287 and Val288. In some poses, Tyr331 also assisted the formation of van der Waals interactions with either the 3-aminopropyl (**7a**) and/or 3-(diethylamino)propyl (**7c**) groups.

The consensus binding mode described above was scored better in eqBChE than in hBChE (see Supplementary Material Figs. S12–S15). This seems to be opposite to the larger inhibitory potency found for compound **7c** (IC_{50} s of 105 and 2.3 nM in eqBChE and hBChE, respectively; Table 1). Nevertheless, caution is necessary due to the well-known limitations of docking calculations, especially regarding the use of rigid templates for the protein, which may be relevant due to the presence of loops at the entrance of the binding pocket, the lack of hydration effects, and the accuracy of the scoring functions [55,56].

Refinement of the selected poses in the different systems was accomplished by means of MD simulations (see Supplementary Material Table S3). Regarding hBChE systems, the simulations started from the 1POM structure revealed that the ligand exhibits a tendency to be released from the binding cavity, arguing against a stable binding mode. However, MD simulations that were started from the 6QAA system showed that ligands **7a** and especially **7c** attain a stable arrangement in

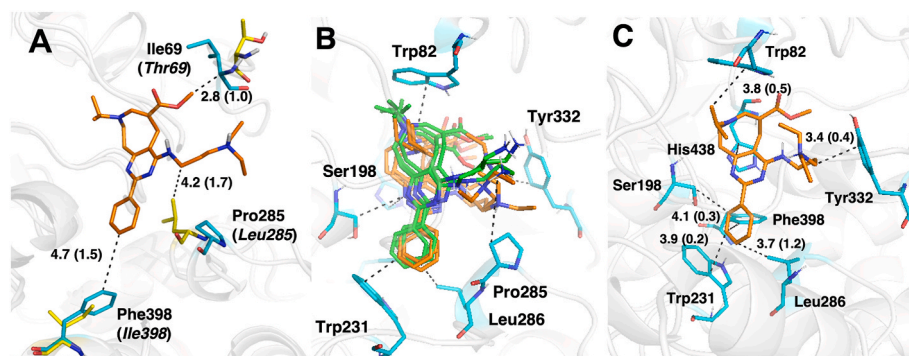


Fig. 4. (A) General arrangement of compound **7c** (C atoms in orange), surrounded by residues (names in brackets) that differ between *hBChE* (C atoms in cyan) and *eqBChE* (C atoms in yellow); averaged distances in Å (SD in parentheses). (B) Superposition of the binding mode of **7a** (C atoms in green) and **7c** (C atoms in orange) at the end of independent MD simulations in the *hBChE* cavity (selected residues in cyan; dashed lines highlight relevant interactions). (C) General arrangement of one replica of compound **7c** (C atoms in orange), surrounded by selected residues in *hBChE* (C atoms in cyan); averaged distances in Å (SD in parentheses).

the binding site, as noted in the time evolution of the root-mean square deviation, which generally varies between 2.0 and 2.5 Å (see [Supplementary Material Fig. S17](#)). The ligands tend to adopt a similar arrangement ([Fig. 4B](#) and [C](#)). In the two cases, both the 3-aminopropyl (**7a**) and 3-(diethylamino)propyl (**7c**) chains present high mobility due to the orientation towards the mouth of the gorge.

Compared to the complexes of **7a** and **7c** with the *hBChE* (6QAA) enzyme, the root-mean square deviation profiles determined for the simulations run for the *eqBChE* systems showed that the ligand exhibits larger fluctuations along the trajectory. Thus, in most cases the root-mean square deviation ranges between 5 and 8 Å (see [Supplementary Material Figs. S18 and S19](#)), suggesting a poorer fitting in the binding pocket of *eqBChE*. Nevertheless, the analysis of the replicas run for *eqBChE* (EQ (1)) points out that the ligands adopt an arrangement similar to the pose found for the *hBChE*, whereas a larger structural diversity is observed in the structures sampled along the *eqBChE* (EQ (2)) simulations.

The most potent *hBChE* inhibitor **7c** tends to place both ethyl groups near Tyr332, at an averaged distance of 3.4 ± 0.2 Å ([Fig. 4C](#)), locating the substituents in a way that shields the charged nitrogen from water molecules. The phenyl group in position 2 is located in the lower part of the cavity, surrounded by Ser198, Trp231, Leu286 and Phe398, at distances ranging between 3.7 ± 1.2 Å and 4.1 ± 0.3 Å ([Fig. 4C](#)). The isopropyl group in position 8, also with high mobility, moves toward to Trp79 (distance close to 3.8 ± 0.5 Å; [Fig. 4C](#)) in the anionic site of the enzyme. Finally, His438 tends to form a π - π stacking interaction with the central pyrimidine ring ([Fig. 4C](#)).

Free energy calculations were performed to determine the binding affinity (ΔG_{bind}) or all human and equine replicas ([Table 5](#)). For the human enzyme, on average **7a** shows an absolute value of -44 kcal/mol, whereas the binding affinity of **7c** is -4.8 kcal/mol more stable. This difference can be attributed to the E_{vdw} component, which is 5 kcal/mol more favorable, thus supporting that the **7c**-*hBChE* complex is more stable. For the equine enzymes, in general all complexes for all replicas are less favored compared to human ones, as the average ΔG_{bind} is decreased by at least 7 kcal/mol, respectively.

The results permit to define a putative binding mode of compounds **7a** and **7c** with *hBChE*, where both ligands exhibit in a similar arrangement along the gorge and the protonated amino group roughly pointing to the entry of the gorge. In view of what was observed in many replicas, this binding mode tends to be stable in the human form. The better activity of **7c** compared to **7a** could be attributed to different aspects mainly related by the addition of the two ethyl groups in **7c**, leading to an enhanced van der Waals interaction with the residues in the binding cavity, and to the shielding effect exerted of both substituents, impeding the access of water molecules.

Despite considering its limitations, our interpretations are supported

Table 5

Contributions to the binding free energy from MM-GBSA calculations (kcal/mol) of **7a** and **7c** bound to *hBChE* and *eqBChE*^a.

Replica	E_{vdw}	E_{elec}	ΔG_{gas}	E_{GB}	E_{SURF}	ΔG_{solv}	ΔG_{bind}
<i>hBChE</i> 6QAA-7a							
R1	-57 ± 3	-154 ± 18	-211 ± 18	173 ± 16	-7 ± 1	166 ± 16	-45 ± 5
R2	-56 ± 3	-151 ± 18	-208 ± 18	171 ± 16	-7 ± 1	164 ± 16	-44 ± 3
R3	-55 ± 2	-137 ± 15	-192 ± 15	155 ± 12	-7 ± 1	149 ± 12	-43 ± 5
<i>hBChE</i> 6QAA-7c							
R1	-62 ± 3	-136 ± 10	-197 ± 10	157 ± 10	-7 ± 2	150 ± 10	-48 ± 3
R2	-63 ± 3	-124 ± 10	-187 ± 11	144 ± 11	-7 ± 2	137 ± 10	-50 ± 3
R3	-66 ± 3	-132 ± 6	-198 ± 7	154 ± 6	-8 ± 2	146 ± 6	-52 ± 3
<i>eqBChE</i> EQ1-7a							
R1	-43 ± 4	-122 ± 22	-165 ± 23	134 ± 19	-5 ± 1	129 ± 19	-36 ± 6
R2	-51 ± 3	-128 ± 20	-180 ± 20	152 ± 17	-6 ± 1	145 ± 17	-34 ± 4
R3	-58 ± 3	-112 ± 12	-170 ± 12	134 ± 12	-7 ± 1	127 ± 12	-42 ± 3
<i>eqBChE</i> EQ1-7c							
R1	-53 ± 4	-105 ± 12	-158 ± 11	130 ± 9	-7 ± 1	123 ± 9	-35 ± 4
R2	-53 ± 3	-115 ± 13	-169 ± 15	136 ± 13	-7 ± 1	129 ± 13	-40 ± 5
R3	-50 ± 4	-68 ± 14	-118 ± 16	92 ± 13	-6 ± 1	85 ± 13	-33 ± 4
<i>eqBChE</i> EQ2-7a							
R1	-49 ± 4	-86 ± 23	-135 ± 23	107 ± 22	-5.45 ± 0.42	102 ± 21	-33 ± 5
R2	-45 ± 3	-97 ± 19	-142 ± 18	121 ± 18	-5.60 ± 0.23	115 ± 18	-27 ± 5
R3	-44 ± 3	-85 ± 17	-129 ± 17	103 ± 15	-5.38 ± 0.44	97 ± 15	-31 ± 4
<i>eqBChE</i> EQ2-7c							
R1	-62 ± 3	-99 ± 6	-160 ± 6	122 ± 5	-8 ± 1	115 ± 5	-45 ± 3
R2	-68 ± 2	-118 ± 7	-186 ± 7	141 ± 6	-8 ± 1	133 ± 6	-53 ± 4
R3	-47 ± 3	-102 ± 14	-149 ± 15	126 ± 14	-6 ± 1	121 ± 14	-29 ± 4

^a Since most of the 1POM simulations tend to skip the cavity, MM-GBSA calculations were not performed.

by MM/GBSA calculations, at least in a qualitative way, as the binding free energy of **7c** is 4–5 kcal/mol more stable than **7a**, in the human form, whereas this difference reduces to 1.5 kcal/mol when equine forms are considered. The main mutations detected between human and

equine forms (Ile69Thr, Ala277Val, Gly283Asp, Pro285Leu and Phe398Ile) could explain the different activity of **7c** between both species. Especially, Pro285Leu is likely the most relevant change, since this residue (in human form) has less conformational flexibility and presumably less clashes with the ligand, than Leu (in equine form), which has a higher degree of conformational freedom. At this point, let us note that these residues are present in a loop with some mobility, as detected in our simulations. Therefore, Leu285 may lead to a higher steric hindrance with **7c**, being detrimental for the profile against equine enzyme.

4. Conclusion

The results of the combined in vitro/in silico study give support to the suitability of the annelated tetrahydroazocine scaffold for developing highly (single-digit nanomolar) potent and selective inhibitors of BChE. The most promising annelated tetrahydroazocine derivative (**7c**) achieved inhibition constant in the low nanomolar range, and a marked selectivity toward BChE. Kinetics studies showed a noncompetitive/mixed-type inhibition mechanism against human BChE, which agrees with the binding mode predicted from molecular docking and molecular dynamics simulations, revealing the congruent arrangement along the gorge leading to the catalytic site, through interactions with residues primarily located along the gorge and the peripheral site. Remarkably, compound **7c**, that did not show any noteworthy inhibitory activity against human MAOs A and B, inhibited P-gp (the efflux pump which hampers the brain permeation of xenobiotics) and showed weak cytotoxicity in the liver HepG2 cell line at concentrations thousands of times higher than the in-vitro IC₅₀ against BChE. Overall, these findings highlight the pivotal role of these molecular determinants in influencing the activity of these compounds, and particularly **7c**, albeit deserving further in-vitro and in-vivo pharmacological assays, emerges as a promising template to design and investigate novel BChE-selective ligands as inhibitors and/or fluorogenic probes in pharmacological applications.

Author statement

I, the undersigned, declare that:

All authors have seen and approved the final version of the manuscript being submitted. The authors confirm that the article is the authors' original work, hasn't received prior publication, and isn't under consideration for publication elsewhere.

All authors have no competing financial interests or personal relationships that could have appeared to influence the work reported in this paper.

Declaration of competing interest

The authors declare the following financial interests/personal relationships which may be considered as potential competing interests: Cosimo D. Altomare reports equipment, drugs, or supplies was provided by University of Bari Department of Pharmacy and Pharmaceutical Sciences.

Data availability

Data will be made available on request.

Acknowledgements

M.d.C., R.P., M.C. and C.D.A. acknowledge the financial support of the Italian Ministry of Education, Universities and Research (PRIN, Grant 201744BNST_004). A.V. and F.J.L. acknowledge financial support from the Spanish Ministerio de Ciencia e Innovación (AEI/10.13039/501100011033; grants PID2020-117646RB-I00 and CEX2021-001202-M), the Generalitat de Catalunya (grant 2021SGR00671). The Consorci

de Serveis Universitaris de Catalunya (CSUC) is acknowledged for computational resources (Molecular Recognition project).

Appendix A. Supplementary data

Supplementary data to this article can be found online at <https://doi.org/10.1016/j.cbi.2023.110741>.

References

- [1] A. Sharma, P. Appukkuttana, E. Van der Eycken, Microwave-assisted synthesis of medium-sized heterocycles, *Chem. Commun.* 48 (11) (2012) 1623–1637, <https://doi.org/10.1039/C1CC15238F>.
- [2] A.V. Listratova, L.G. Voskressensky, Recent advances in the synthesis of hydrogenated azocine-containing molecules, *Synthesis* 49 (17) (2017) 3801–3834, <https://doi.org/10.1055/s-0036-1589500>.
- [3] S. Lee, J. Sperry, Isolation and biological activity of azocine and azocane alkaloids, *Bioorg. Med. Chem.* 54 (2021) 116560–116563, <https://doi.org/10.1016/j.bmc.2021.116560>.
- [4] A. Hussain, S.K. Yousuf, D. Mukherjee, Importance and synthesis of benzannulated medium-sized and macrocyclic rings (BMRs), *RSC Adv.* 4 (2014) 43241–43257, <https://doi.org/10.1039/C4RA07434C>, and references cited therein.
- [5] S. Lee, J. Sperry, M.S. Novikov, E.Y. Shinkevich, D. Vidovic, Selective transannular ring transformations in azirino-fused eight-membered O,N- or S, N-heterocycles, *Org. Biomol. Chem.* 21 (2005) 4040–4042, <https://doi.org/10.1039/B512409C>, 2005.
- [6] A. Carotti, M. de Candia, M. Catto, T.N. Borisova, A.V. Varlamov, E. Méndez-Alvarez, R. Soto-Otero, L.G. Voskressensky, C.D. Altomare, Ester derivatives of annelated tetrahydroazocines: a new class of selective acetylcholinesterase inhibitors, *Bioorg. Med. Chem.* 14 (21) (2006) 7205–7212, <https://doi.org/10.1016/j.bmc.2006.06.055>.
- [7] A.A. Titov, R. Purgatorio, A.Y. Obydenik, A.V. Listratova, T.N. Borisova, M. de Candia, M. Catto, C.D. Altomare, A.V. Varlamov, L.G. Voskressensky, Synthesis of isomeric 3-Benzazocines decorated with endocyclic allene moiety and exocyclic conjugated double bond and evaluation of their anticholinesterase activity, *Molecules* 27 (19) (2022) 6276, <https://doi.org/10.3390/molecules27196276>.
- [8] M.S. Kobzev, A.A. Titov, E.V. Alexandrova, R. Purgatorio, M. Catto, E.A. Sorokina, T.N. Borisova, A.V. Varlamov, C.D. Altomare, L.G. Voskressensky, Synthesis of 8-phenyl substituted 3-benzazocines with allene moiety, their thermal rearrangement and evaluation as acetylcholinesterase inhibitors, *Mol. Divers.* 26 (2) (2022) 1243–1247, <https://doi.org/10.1007/s11030-021-10185-8>.
- [9] A.A. Titov, M.S. Kobzev, M. Catto, M. de Candia, N. Gambacorta, N. Denora, L. Pisani, O. Nicolotti, T.N. Borisova, A.V. Varlamov, L.G. Voskressensky, C. D. Altomare, Away from flatness: unprecedented nitrogen-bridged cyclopenta[a]indene derivatives as novel anti-alzheimer multitarget agents, *ACS Chem. Neurosci.* 12 (2) (2021) 340–353, <https://doi.org/10.1021/acscchemneuro.0c00706>.
- [10] J. Jasiński, A. Szczoczarz, D. Cysewski, K. Lewandowski, P. Skowron, K. Waleron, B. Wasag, Butyrylcholinesterase-protein interactions in human serum, *Int. J. Mol. Sci.* 22 (19) (2021), 10662, <https://doi.org/10.3390/ijms221910662>.
- [11] O. Lockridge, Review of human butyrylcholinesterase structure, function, genetic variants, history of use in the clinic, and potential therapeutic uses, *Pharmacol. Ther.* 148 (2015) 34–46, <https://doi.org/10.1016/j.pharmthera.2014.11.011>.
- [12] E.M. Scott, R.F. Powers, Human serum cholinesterase, a tetramer, *Nat. New Biol.* 236 (64) (1972) 83–84, <https://doi.org/10.1038/newbio236083a0>.
- [13] J. Jasiński, B. Wasag, Butyrylcholinesterase protein ends in the pathogenesis of Alzheimer's disease - could BChE genotyping be helpful in Alzheimer's therapy? *Biomolecules* 9 (10) (2019) 592, <https://doi.org/10.3390/biom9100592>.
- [14] P. Gómez-Ramos, C. Bouras, M.A. Morán, Ultrastructural localization of butyrylcholinesterase on neurofibrillary degeneration sites in the brains of aged and Alzheimer's disease patients, *Brain Res.* 640 (1–2) (1994) 17–24, [https://doi.org/10.1016/0006-8993\(94\)91852-x](https://doi.org/10.1016/0006-8993(94)91852-x).
- [15] O. Lockridge, L.M. Schopfer, G. Winger, J.H. Woods, Large scale purification of butyrylcholinesterase from human plasma suitable for injection into monkeys; a potential new therapeutic for protection against cocaine and nerve agent toxicity, *J. Med. Chem. Biol. Radiol. Def.* 3 (2005), nihms5095, <https://doi.org/10.1901/jaba.2005.3-nihms5095>.
- [16] P. Masson, O. Lockridge, Butyrylcholinesterase for protection from organophosphorus poisons: catalytic complexities and hysteretic behavior, *Arch. Biochem. Biophys.* 494 (2) (2010) 107–120, <https://doi.org/10.1016/j.abb.2009.12.005>.
- [17] C.E. Mattes, T.J. Lynch, A. Singh, R.M. Bradley, P.A. Kellaris, R.O. Brady, K. L. Dretchen, Therapeutic use of butyrylcholinesterase for cocaine intoxication, *Toxicol. Appl. Pharmacol.* 145 (2) (1997) 372–380, <https://doi.org/10.1006/taap.1997.8188>.
- [18] M.W.D. Thorne, M.K. Cash, G.A. Reid, D.E. Burley, D. Luke, I.R. Pottie, S. Darvesh, Imaging butyrylcholinesterase in multiple sclerosis, *Mol. Imag. Biol.* 23 (1) (2021) 127–138, <https://doi.org/10.1007/s11307-020-01540-6>.
- [19] S. Brimijoin, V.P. Chen, Y.P. Pang, L. Geng, Y. Gao, Physiological roles for butyrylcholinesterase: a BChE-ghrelin axis, *Chem. Biol. Interact.* 259 (Pt B) (2016) 271–275, <https://doi.org/10.1016/j.cbi.2016.02.013>.
- [20] L.G. Voskressensky, S.V. Akbulatov, T.N. Borisova, A.V. Varlamov, A novel synthesis of hexahydroazonoindoles using activated alkynes in an azepine ring

- expansion, *Tetrahedron* 62 (52) (2006) 12392–12397, <https://doi.org/10.1016/j.tet.2006.09.107>.
- [21] L.G. Voskressensky, S.V. Akbulatov, T.N. Borisova, A.V. Kleimenov, A.V. Varlamov, Synthesis of hexahydroazono[5,6-*b*]indoles from hexahydroazepino[4,3-*b*]and-[3,4-*b*]indoles and activated alkynes, *Russ. Chem. Bull.* 56 (11) (2007) 2323–2329, <https://doi.org/10.1007/s11172-007-0367-7>.
- [22] L.G. Voskressensky, T.N. Borisova, A.V. Listratova, L.N. Kulikova, A.A. Titov, A. V. Varlamov, Tandem enlargement of the tetrahydropyridine ring in 1-aryl-tetrahydroisoquinolines using activated alkynes—a new and effective synthesis of benzoazocines, *Tetrahedron Lett.* 47 (27) (2006) 4585–4589, <https://doi.org/10.1016/j.tetlet.2006.04.151>.
- [23] L.G. Voskressensky, A.V. Listratova, T.N. Borisova, G.G. Alexandrov, A. V. Varlamov, Synthesis of benzoazocines from substituted tetrahydroisoquinolines and activated alkynes in a tetrahydropyridine ring expansion, *Eur. J. Org. Chem.* 36 (36) (2007) 6106–6117, <https://doi.org/10.1002/ejoc.200700602>.
- [24] L.G. Voskressensky, T.N. Borisova, I.S. Kostenev, L.N. Kulikova, A.V. Varlamov, Tetrahydropyridine (THP) ring expansion under the action of activated terminal alkynes. The first synthesis and X-ray crystal structure of tetrahydropyrimido[4,5-*d*]azocines, *Tetrahedron Lett.* 47 (6) (2006) 999–1001, <https://doi.org/10.1016/j.tetlet.2005.11.136>.
- [25] L.G. Voskressensky, M.V. Ovcharov, T.N. Borisova, L.N. Kulikova, A.V. Listratova, V.S. Borisov, A.V. Varlamov, 2-Alkyl-4-oxohexahydropyrimido[4,5-*d*]azocines, *Chem. Heterocycl. Compd.* 47 (2) (2011) 222–228, <https://doi.org/10.1007/s10593-011-0744-x>.
- [26] L.G. Voskressensky, M.V. Ovcharov, T.N. Borisova, A.V. Listratova, L.N. Kulikova, E.A. Sorokina, S.P. Gromov, A.V. Varlamov, Synthesis of 4-amino-substituted tetrahydropyrimido[4,5-*d*]azocines, *Chem. Heterocycl. Compd.* 49 (8) (2013) 1180–1187, <https://doi.org/10.1007/s10593-013-1361-7>.
- [27] M. de Candia, P. Fossa, S. Cellamare, L. Mosti, A. Carotti, C.D. Altomare, Insights into structure-activity relationships from lipophilicity profiles of pyridin-2(1*H*)-one analogs of the cardiotonic agent milrinone, *Eur. J. Pharmaceut. Sci.* 26 (1) (2005) 78–86, <https://doi.org/10.1016/j.ejps.2005.05.001>.
- [28] K. Takacs-Novak, K.J. Box, A. Avdeev, Potentiometric pK_a determination of water-insoluble compounds. Validation study in methanol/water mixtures, *Int. J. Pharm.* 151 (2) (1997) 235–248, [https://doi.org/10.1016/S0378-5173\(97\)04907-7](https://doi.org/10.1016/S0378-5173(97)04907-7).
- [29] B.D. Belviso, R. Caliendo, M. de Candia, G. Zaetta, G. Lopopolo, F. Incampo, M. Colucci, C.D. Altomare, How a β-D-glucoside side chain enhances binding affinity to thrombin of inhibitors bearing 2-chlorothiophene as P1 moiety: crystallography, fragment deconstruction study, and evaluation of antithrombotic properties, *J. Med. Chem.* 57 (20) (2014) 8563–8575, <https://doi.org/10.1021/jm5010754>.
- [30] A.A. Nevskaya, M.D. Matveeva, T.N. Borisova, M. Niso, N.A. Colabufo, A. Boccarelli, R. Purgatorio, M. de Candia, S. Cellamare, L.G. Voskressensky, C. D. Altomare, A new class of 1-Aryl-5,6-dihydroazepino[2,1-*a*]isoquinoline derivatives as reversers of P-Glycoprotein-Mediated multidrug resistance in tumor cells, *ChemMedChem* 13 (15) (2018) 1588–1596, <https://doi.org/10.1002/cmdc.201800177>.
- [31] R. Purgatorio, M. de Candia, M. Catto, M. Rullo, L. Pisani, N. Denora, A. Carrieri, A. A. Nevskaya, L.G. Voskressensky, C.D. Altomare, Evaluation of water-soluble mannich base prodrugs of 2,3,4,5-Tetrahydroazepino[4,3-*b*]indol-1(6*H*)-one as multitarget-directed agents for Alzheimer's disease, *ChemMedChem* 16 (3) (2021) 589–598, <https://doi.org/10.1002/cmdc.202000583>.
- [32] R. Purgatorio, L.N. Kulikova, L. Pisani, M. Catto, M. de Candia, A. Carrieri, S. Cellamare, A. De Palma, A.A. Beloglazkin, G. Reza Raesi, L.G. Voskressensky, C. D. Altomare, Scouting around 1,2,3,4-tetrahydrochromeno[3,2-*c*]pyridin-10-ones for single- and multitarget ligands directed towards relevant Alzheimer's targets, *ChemMedChem* 15 (20) (2020) 1947–1955, <https://doi.org/10.1002/cmdc.202000468>.
- [33] R. Purgatorio, M. de Candia, A. De Palma, F. De Santis, L. Pisani, F. Campagna, S. Cellamare, C.D. Altomare, M. Catto, Insights into structure-activity relationships of 3-arylhydrazonoindolin-2-one derivatives for their multitarget activity on β-amyloid aggregation and neurotoxicity, *Molecules* 23 (7) (2018) 1544, <https://doi.org/10.1002/cmdc.202000468>.
- [34] Y. Nicolet, O. Lockridge, P. Masson, J.C. Fontecilla-Camps, F. Nachon, Crystal structure of human butyrylcholinesterase and of its complexes with substrate and products, *J. Biol. Chem.* 278 (42) (2003) 41141–41147, <https://doi.org/10.1074/jbc.M210241200>.
- [35] A. Meden, D. Knez, M. Jukic, X. Brazzalotto, M. Grsic, A. Pisljar, A. Zahirovic, J. Kos, F. Nachon, J. Svete, S. Gobec, U. Groselj, Tryptophan-derived butyrylcholinesterase inhibitors as promising leads against Alzheimer's disease, *Chem. Commun.* 55 (26) (2019) 3765–3768, <https://doi.org/10.1039/c9cc01330j>.
- [36] M. Johnson, I. Zaretskaya, Y. Raytselis, Y. Merezuk, S. McGinnis, T.L. Madden, NCBI BLAST: a better web interface, *Nucleic Acids Res.* 36 (2008) W5–W9, <https://doi.org/10.1093/nar/gkn201> (web server issue).
- [37] A. Waterhouse, M. Bertoni, S. Bienert, G. Studer, G. Tauriello, R. Gumienny, F. T. Heer, T.A.P. de Beer, C. Rempfer, L. Bordoli, R. Lepore, T. Schwede, SWISS-MODEL: homology modelling of protein structures and complexes, *Nucleic Acids Res.* 46 (W1) (2018) W296–W303, <https://doi.org/10.1093/nar/gky427>.
- [38] Schrödinger Release 2021-2: Glide, Schrödinger, LLC, New York, NY, 2021.
- [39] D.A. Case, K. Belfon, I.Y. Ben-Shalom, S.R. Brozell, D.S. Cerutti, T.E. III Cheatham, V.W.D. Cruzeiro, T.A. Darden, R.E. Duke, G. Giambasu, M.K. Gilson, H. Gohlke, A. W. Goetz, R. Harris, S. Izadi, S.A. Izmailov, K. Kasavajhala, A. Kovalenko, R. Krasny, T. Kurtzman, T.S. Lee, S. LeGrand, P. Li, C. Lin, J. Liu, T. Luchko, R. Luo, V. Man, K.M. Merz, Y. Miao, O. Mikhailovskii, G. Monard, H. Nguyen, A. Onufriev, F. Pan, S. Pantano, R. Qi, D.R. Roe, A. Roitberg, C. Sagui, S. Schott-Verdugo, J. Shen, C.L. Simmerling, N.R. Skrynnikov, J. Smith, J. Swails, R.C. Walker, J. Wang, L. Wilson, R.M. Wolf, X. Wu, Y. Xiong, Y. Xue, D.M. York, P.A. Kollman, AMBER 2020, University of California, San Francisco.
- [40] K. Lindorff-Larsen, S. Piana, K. Palmo, P. Maragakis, J.L. Klepeis, R.O. Dror, D. E. Shaw, Improved side-chain torsion potentials for the Amber ff99SB protein force field, *Proteins* 78 (8) (2010) 1950–1958, <https://doi.org/10.1002/prot.22711>.
- [41] J. Wang, R.M. Wolf, J.K. Caldwell, P.A. Kollman, D.A. Case, Development and testing of a general AMBER force field, *J. Comput. Chem.* 25 (9) (2004) 1157–1174, <https://doi.org/10.1002/jcc.20035>.
- [42] C.I. Bayly, P. Cieplak, W. Cornell, P.A. Kollman, A well-behaved electrostatic potential based method using charge restraints for deriving atomic charges: the RESP model, *J. Phys. Chem.* 97 (40) (1993) 10269–10280, <https://doi.org/10.1021/j100142a004>.
- [43] W.L. Jorgensen, J. Chandrasekhar, J.D. Madura, R.W. Impey, M.L. Klein, Comparison of simple potential functions for simulating liquid water, *J. Chem. Phys.* 79 (2) (1983) 926–935, <https://doi.org/10.1063/1.445869>.
- [44] J.-P. Ryckaert, G. Cicotti, H.J.C. Berendsen, Numerical integration of the cartesian equations of motion of a system with constraints: molecular dynamics of n-alkanes, *J. Comput. Phys.* 23 (3) (1977) 327–341, [https://doi.org/10.1016/0021-9991\(77\)90098-5](https://doi.org/10.1016/0021-9991(77)90098-5).
- [45] T. Darden, D. York, L. Pedersen, Particle Mesh Ewald: an N-log(N) method for Ewald sums in large systems, *J. Chem. Phys.* 98 (12) (1993) 10089–10092, <https://doi.org/10.1063/1.464397>.
- [46] S. Genheden, U. Ryde, The MM/PBSA and MM/GBSA methods to estimate ligand-binding affinities, *Expert Opin. Drug Discov.* 10 (5) (2015) 449–461, <https://doi.org/10.1517/17460441.2015.1032936>.
- [47] P.D. Bailey, S.P. Hollinshead, Application of a modified Pictet–Spengler reaction to the synthesis of optically active tetrahydro-β-carbolines, key intermediates in the preparation of many indole alkaloids, *J. Chem. Soc., Perkin Trans. 1* (4) (1988) 739–745, <https://doi.org/10.1039/P19880000739>.
- [48] L.G. Voskressensky, T.N. Borisova, L.N. Kulikova, E.G. Dolgova, A.I. Kleimenov, E. A. Sorokina, A.A. Titov, A.V. Varlamov, Reaction of 1-substituted tetrahydro-β-carbolines with activated alkynes—a new original approach to the synthesis of tetrahydroazocino[5,4-*b*]indoles Chem, *Heterocycl. Compd.* 43 (5) (2007) 587–598, <https://doi.org/10.1007/s10593-007-0093-y>.
- [49] G.R. Clemp, D.G.I. Felton, 151. The chemistry of the carbazoles. 1 : 2 : 3 : 4-tetrahydro-4-ketocarbazoles, *J. Chem. Soc.* (1951) 700–703, <https://doi.org/10.1039/JR9510000700>, 0.
- [50] J.B. Hester Jr., Azepinoindoles. II. 1,2,3,4,5,6-Hexahydroazepino[3,2-*b*]indole and 1,2,3,4,5,6-hexahydroazepino[4,3-*b*]indole, *J. Org. Chem.* 32 (12) (1967) 3804–3808, <https://doi.org/10.1021/jo01287a017>.
- [51] L.N. Kulikova, R.S. Borisov, L.G. Voskressensky, Ring opening in 1,2,3,4-tetrahydrochromeno[3,2-*c*]pyridines under the action of electron-deficient alkynes, *Mendeleev Commun.* 27 (6) (2017) 640–641, <https://doi.org/10.1016/j.mencom.2017.11.035>.
- [52] B. Feng, A.C. Doran, L. Di, M.A. West, S.M. Osgood, J.Y. Mancuso, C.L. Shaffer, Tremaine, J. Liras, Prediction of human brain penetration of P-glycoprotein and breast cancer resistance protein substrates using in vitro transporter studies and animal models, *J. Pharmaceut. Sci.* 107 (8) (2018) 2225–2235, <https://doi.org/10.1016/j.xphs.2018.03.018>.
- [53] L.C. Tan, P.W. Carr, Extra-thermodynamic relationships in chromatography-study of the relationship between the slopes and intercepts of plots of log k' vs. mobile phase composition in reversed-phase chromatography, *J. Chromatogr., A* 656 (1–2) (1993) 521–535, [https://doi.org/10.1016/0021-9673\(93\)80817-R](https://doi.org/10.1016/0021-9673(93)80817-R).
- [54] G. Parisi, L. Degennaro, C. Carlucci, M. de Candia, P. Mastorilli, A. Roller, W. Holzer, C.D. Altomare, V. Pace, R. Luisi, A greener and efficient access to substituted four- and six-membered sulfur-bearing heterocycles, *Org. Biomol. Chem.* 15 (23) (2017) 5000–5015, <https://doi.org/10.1039/c7ob00846e>.
- [55] C.N. Cavasotto, M.G. Aucar, N.S. Adler, Computational chemistry in drug lead discovery and design, *Int. J. Quant. Chem.* 119 (2) (2019), e25678, <https://doi.org/10.1002/qua.25678>.
- [56] I.A. Guedes, F.S.S. Pereira, L.E. Dardenne, Empirical scoring functions for structure-based virtual screening: applications, critical aspects, and challenges, *Front. Pharmacol.* 9 (2018) 1089, <https://doi.org/10.3389/fphar.2018.01089>.